Andean Geology 52 (1): 1-46. January, 2025 doi: 10.5027/andgeoV52n1-3689

Lithofacies architecture within an intra-arc environment: A case study from the Permian-Triassic magmatic arc in the Chilean Frontal Cordillera (30-30.5° S)

*Diego Castillo¹, Ismael Murillo², Verónica Oliveros^{1,3}

- Departamento Ciencias de la Tierra, Universidad de Concepción, Edmundo Larenas 129, Casilla 160-C, Concepción, Chile. dicastilloherrera@gmail.com, voliveros@udec.cl
- ² Servicio Nacional de Geología y Minería (Sernageomin), Av. Santa María 0104, Santiago, Chile. ismael.murillo@sernageomin.cl
- ³ Millenium Institute of Volcanic Risk Research-Ckelar Volcanoes, Av. Angamos 0610, Antofagasta, Chile.

ABSTRACT. In the Chilean Frontal Cordillera between 28.5 and 30.5° S, two volcano-sedimentary succesions of Late Guadalupian to Middle Triassic age croup out: the El Tapado (Late Guadalupian-Lopingian) and Guanaco Sonso (Late Lopingian-Middle Triassic) formations, representing the westernmost exposures of the Choiyoi Group and post-Choiyoi magmatism. Recently, these two units have been characterized in detail, shedding light into the tectonic and climatic context of the late stages of the Choiyoi magmatism, and, more generally, the geology of intra-arc successions in the southwestern Gondwana margin. In this work, we present a stratigraphy and lithofacies analysis of three stratigraphic sections studied in the La Laguna sector (30-30.5° S), comprising rocks of the El Tapado and Guanaco Sonso formations. The former is dominated by caldera-related rhyolitic to dacitic ignimbrites accumulated in depocenters associated with the extensional activity of major structures. Lacustrine and fluvial-alluvial deposits interbedded in this rock unit were mainly controlled by volcaniclastic input and subsidence dynamics, and record the transition from relatively humid conditions to semi-arid or even arid conditions during the Late Guadalupian-Lopingian, consistent with regional paleoclimatic observations. On the other hand, the Guanaco Sonso Formation presents mainly intermediate, proximal (near-vent) volcanic products that denote a varied volcanism in terms of composition and eruptive style, likely controlled by structures and tectonics. We conclude the southwestern Gondwana margin sustained high-explosivity, silicic volcanism (El Tapado) that transitioned into a more varied, mainly intermediate volcanism (Guanaco Sonso). This activity ultimately gave way to the basaltic-andesitic to bimodal products that characterized the final part of the pre-Andean stage during the Triassic in this region.

Keywords: El Tapado Formation, Guanaco Sonso Formation, Lithofacies associations, Chilean Frontal Cordillera, Choiyoi Group.

RESUMEN. Arquitectura de litofacies en un ambiente de intrarco: un caso de estudio en el arco magmático Pérmico-Triásico de la Cordillera Frontal chilena (30-30,5° S). En la Cordillera Frontal chilena, entre los 28,5 y 30,5° S, afloran dos sucesiones volcanosedimentarias de edad guadalupiana tardía a triásica media: las formaciones El Tapado (Guadalupiano tardío-Lopingiano) y Guanaco Sonso (Lopingiano tardío-Triásico medio), que representan las exposiciones más occidentales del Grupo Choiyoi así como del magmatismo post-Choiyoi. Estas dos unidades han sido recientemente caracterizadas en detalle, lo que esclarece el contexto tectónico y climático de las últimas etapas del magmatismo Choiyoi y, más en general, la geología de las sucesiones de intrarco en el margen suroccidental de Gondwana. En este trabajo se presenta un análisis estratigráfico y de litofacies de tres secciones estratigráficas

^{*} Corresponding author: dicastilloherrera@gmail.com

estudiadas en el sector La Laguna (30-30,5° S), que comprenden rocas de las formaciones El Tapado y Guanaco Sonso. La primera está dominada por ignimbritas riolíticas a dacíticas asociadas a calderas, acumuladas en depocentros generados por actividad tectónica extensional. Los depósitos lacustres y fluvioaluviales intercalados en esta unidad estuvieron controlados principalmente por los aportes volcanoclásticos y la dinámica de subsidencia, y registran la transición de condiciones climáticas relativamente húmedas a condiciones semiáridas o incluso áridas durante el Guadalupiano tardío-Lopingiano, consistente con observaciones paleoclimáticas regionales. Por otro lado, la Formación Guanaco Sonso presenta productos volcánicos proximales (*i.e.*, cercanos a los centros de emisión) y de composición intermedia, lo cual denota un volcanismo variado en términos de composición y estilo eruptivo, probablemente controlado por estructuras y tectonismo. Se concluye que el volcanismo silícico de alta explosividad observado en la Formación El Tapado evolucionó a una actividad volcánica más variada, principalmente intermedia, representada por la Formación Guanaco Sonso. Esta actividad finalmente dio paso a los productos andesítico-basálticos a bimodales que caracterizaron la parte final de la etapa pre-Andina durante el Triásico en la región.

Palabras clave: Formación El Tapado, Formación Guanaco Sonso, Asociaciones de litofacies, Cordillera Frontal chilena, Grupo Choiyoi.

1. Introduction

The Permian-Triassic evolution of the southwestern Gondwana margin (present-day South America) is marked by the widespread volcanism associated with the Choiyoi Magmatic Province (Sato et al., 2015). This continental-scale province is equivalent in volume to silicic large igneous provinces (SLIPs) worldwide, but its magmatic products are less silicic than common SLIPs (Bastías-Mercado et al., 2020). The geotectonic setting that promoted the Choiyoi magmatism is contentious, and it could correspond to either a non-convergent margin with orogenic collapse/slab breakoff (Mpodozis and Kay, 1992; Gianni and Navarrete, 2022) or to an active subduction zone (Rocher et al., 2015). Whereas the extension and composition of the igneous units that crop out in Argentina make them difficult to reconcile with a subduction zone magmatism, detailed geological, petrographic, and geochemical studies carried out in Chile and some areas of Argentina (Rocher et al., 2015) provide evidence that subduction is the most likely setting for the observed magmatism (e.g., del Rey et al., 2016; Coloma et al., 2017; González et al., 2018; Oliveros et al., 2020).

The geological evolution of the Choiyoi Group is also important in terms of the long-term climate effects caused by its protracted, highly explosive volcanic activity, whose deposits can be found along >3,000 km of the South American continental margin (Bastías-Mercado *et al.*, 2020, and references therein). In fact, it has been suggested that the sedimentary substratum in which the magmatic activity took place may have triggered significant atmospheric compositional changes, inducing a climate response on a continental, if not global, scale (Spalletti and

Limarino, 2017). Prior studies related the Permian to Early Triassic volcano-sedimentary sequences and plutonic rocks of the Frontal Cordillera in Chile to the Choiyoi Group, particularly based on their lithological, geochemical, and geochronological characteristics (Maksaev et al., 2014; Sato et al., 2015; Velásquez et al., 2021). However, scarce sedimentary rock records of Permian age have so far been reported from Chile, and thus little is known about the paleoenvironmental context of the Choyoi Group at the continent's edge. In addition, even though the Chilean Frontal Cordillera between 28.5 and 30.5° S provides excellent outcrops for the study of the Choiyoi-related igneous and sedimentary rocks (Fig. 1), the remoteness of this area has hampered the development of detailed stratigraphic and sedimentological studies, with remarkable exceptions involving Triassic rocks at ~29° S (López et al., 2015; Salazar and Coloma, 2016).

The recently discovered Permian to Triassic volcano-sedimentary section exposed in the La Laguna sector (30-30.5° S; Figs. 1 and 2; Velásquez et al., 2021), provides an unprecedented, almost continuous record of ~30 Myr of volcanic and sedimentary activity within an intra-arc environment in the outboard of SW Gondwana, penecontemporaneous to the Choiyoi magmatism. In consequence, this work attempts to unravel the roles of volcanism, sedimentation, and tectonism behind the facies architecture of these rocks, in order to establish a solid relationship with the Choiyoi Group at around the 30-30.5° S latitude segment. Complementary insights into the paleoenvironmental evolution of the observed intra-arc setting as well as possible paleoclimatic controls in the sedimentary record of the study area (cf. Limarino et al., 2014) will also

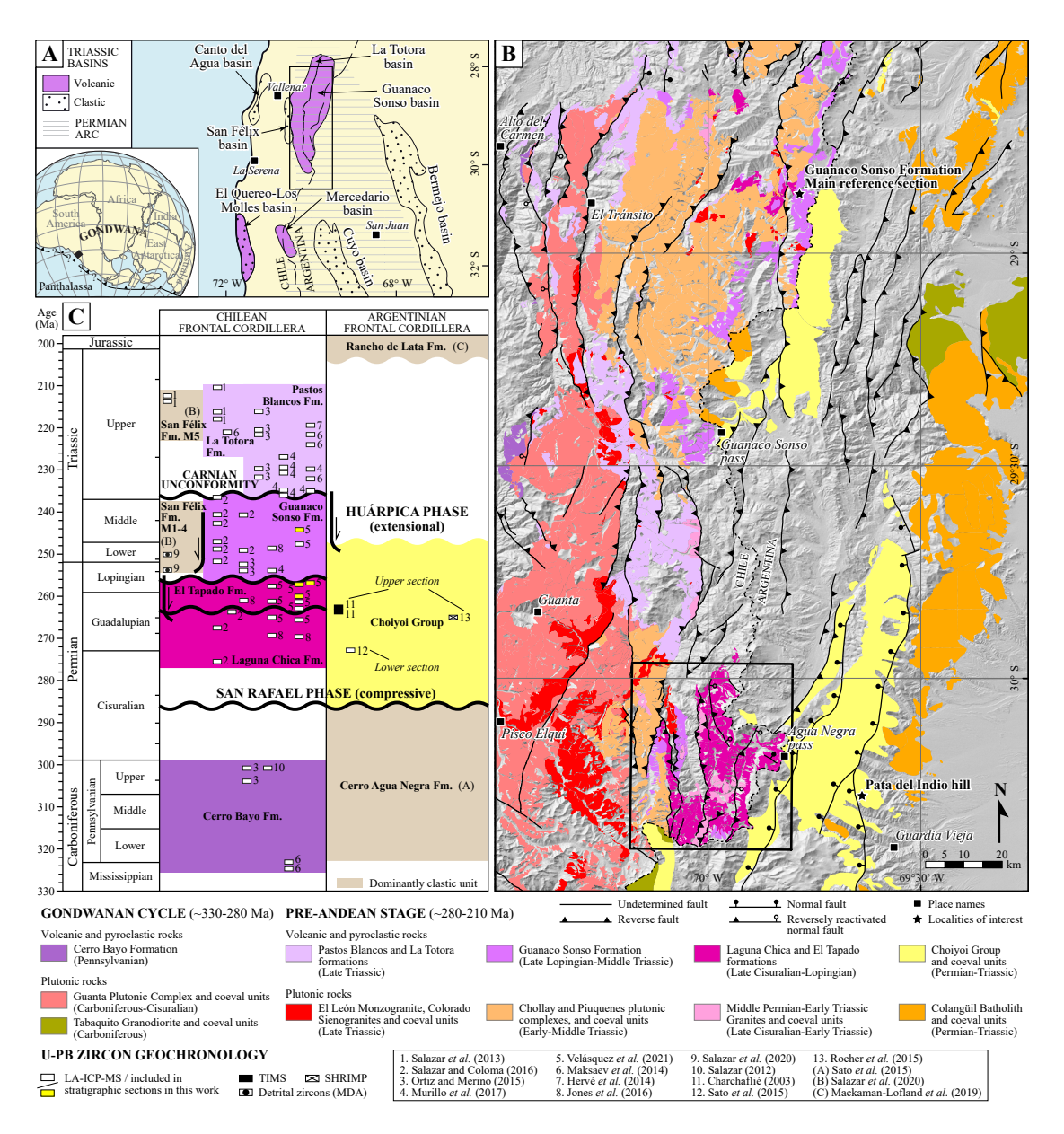


FIG. 1. Location and regional geological context of the study area. A. Position on the southwestern margin of Gondwana and tectonosedimentary context of the study area (modified from Salazar et al., 2020). The box encloses the area of figure 1B. B. Outcrops of Gondwanan and pre-Andean magmatism in the Frontal Cordillera between 28°30'S and 30°30'S. The geological information comes from 1:100,000 scale mapping by Sernageomin in Chile (Salazar et al., 2013; Ortiz and Merino, 2015; Salazar and Coloma, 2016; Murillo et al., 2017; Velásquez et al., 2021), and 1:250,000 scale mapping by Segemar in Argentina (Cardó et al., 2005, 2007; Cravero et al. (2009)). The box encloses the study area. C. Geochronology of Gondwanan and pre-Andean volcanism in the Frontal Cordillera between 28-32° S.

be provided. Finally, the volcanic evolution of the study area during the Triassic will be compared with that observed at ~29° S in Chilean territory to check for regional consistencies.

As a foundation for this work, this research presents a detailed stratigraphic characterization and lithofacies analysis, together with the structural and geochronological controls, of two volcano-sedimentary

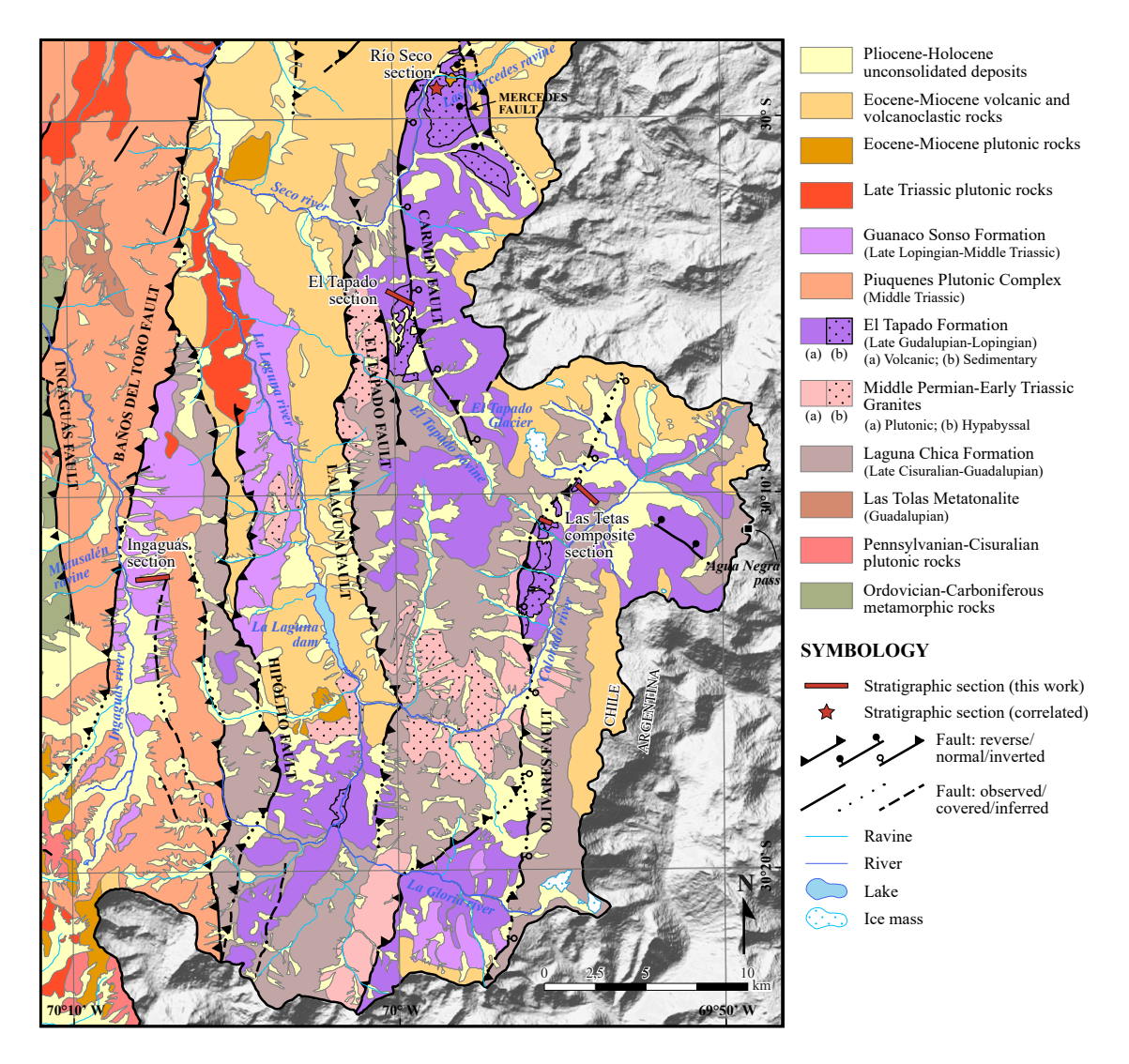


FIG. 2. Geological map of the study area (see figure 1B for location). The stratigraphic sections of this work are indicated, together with a correlated section of Murillo *et al.* (2017) (see Section 5). Figure modified from Murillo *et al.* (2017) and Velásquez *et al.* (2021).

units of Late Guadalupian to Middle Triassic age exposed in the La Laguna sector. The results build on Castillo (2021), which was carried out together with the Pisco Elqui and Paso del Agua Negra 1:100,000-scale geological map published by Sernageomin in 2021 (Velásquez *et al.*, 2021).

2. Geological setting

The Paleozoic and Early Mesozoic tectonic evolution of the southwestern margin of Pangea/Gondwana comprises, at least, the Gondwanan

(Carboniferous to Early Cisuralian) and Andean (Rhaetian to Early Cretaceous) cycles, with the pre-Andean (Middle Cisuralian to Norian) stage in between (sensu Oliveros et al., 2020). The Gondwanan and Early Andean cycles are periods of contrasting plate convergence conditions (e.g., Charrier et al., 2007; Oliveros et al., 2020). The geotectonic setting of the pre-Andean stage, which marked the final assembly of Gondwana and the onset of the conditions that eventually led to its breakup (e.g., Charrier et al., 2007), is more contentious, but recent evidence strongly supports

it involved subduction and the development of a magmatic arc (del Rey *et al.*, 2016; Coloma *et al.*, 2017; Espinoza *et al.*, 2019; Oliveros *et al.*, 2020).

In the Frontal Cordillera of Chile between 28.5 and 30.5° S, the Late Cisuralian-Lopingian magmatic arc is represented by the dominantly rhyolitic to dacitic pyroclastic and lava successions of the Laguna Chica and the El Tapado formations (Salazar and Coloma, 2016; Velásquez et al., 2021) (Fig. 1), associated with high-volume, explosive volcanic eruptions. The Late Cisuralian-Guadalupian Laguna Chica Formation comprises mainly dacitic to rhyolitic ash tuffs and lapilli-ash tuffs, with a few lavas and volcaniclastic sandstone lenses (Salazar and Coloma, 2016; Velásquez et al., 2021). The Late Guadalupian-Lopingian El Tapado Formation unconformably overlies the Laguna Chica Formation and has two lithofacies associations (Fig. 2): a dominant pyroclastic one of rhyolitic to dacitic lapilli-ash tuffs to ash-lapilli tuffs and subordinated intermediate to basic lavas, and a sedimentary one of limestones, sandstones, tuffites, and evaporites (Velásquez et al., 2021). Plutonism during this period is associated with the Las Tolas Metatonalite (~270 Ma), interpreted as a syn-to-post tectonic pluton developed in the latest stages of the San Rafael orogenic phase (Velásquez et al., 2021). More broadly, the plutonic and hypabyssal intrusive rocks of Middle Permian to Early Triassic age are closely related, and partially intrude, the coeval volcanic formations (Salazar and Coloma, 2016; Velásquez et al., 2021).

The Late Lopingian-Middle Triassic arc is represented by the widely extended Guanaco Sonso Formation (Salazar and Coloma, 2016) and voluminous acid intrusive rocks of the Chollay (Salazar and Coloma, 2016) and Piuquenes (Velásquez *et al.*, 2021) plutonic complexes, which partially intrude it (Figs. 1 and 2). The Guanaco Sonso Formation, which unconformably overlies the El Tapado Formation, comprises ignimbrites, tuffaceous breccias, and lavas ranging from dacitic to andesitic in composition, together with subordinate sedimentary intercalations, and has been associated with high explosivity, calderaforming eruptions (López *et al.*, 2015; Salazar and Coloma, 2016; Velásquez *et al.*, 2021).

The Late Triassic volcanism is marked by lava and pyroclastic basaltic to rhyolitic rocks of the Pastos Blancos and the La Totora formations, whereas plutonism is markedly granitic (Salazar *et al.*, 2013; Ortiz and Merino, 2015; Salazar *et al.*, 2020; Velásquez *et al.*, 2021) (Fig. 1).

In the Frontal Cordillera of Argentina, the Permian-Early Triassic volcanism is predominantly represented by the Choiyoi Group, characterized by an andesitic to dacitic lower section and a dominantly rhyolitic upper section, which overlay folded sedimentary turbidites of the Cerro Agua Negra Formation (Sato and Llambías, 1993; Heredia *et al.*, 2002). The intrusive equivalents of the Choiyoi Group consist mainly of granodioritic and granitic rocks grouped into the Colangüil Batholith (Llambías *et al.*, 1993; Sato *et al.*, 2015). Post-Choiyoi volcanism is represented by thin volcanic and pyroclastic deposits interlayered in Triassic sediments (Sato *et al.*, 2015).

During the pre-Andean stage, an extensional structural regime likely prevailed in the southwestern margin of Gondwana, as suggested by different studies in Argentina on rocks of the Choiyoi Group that show numerous normal faults controlling variations in thickness and distribution of deposits at local and regional scales (e.g., Heredia et al., 2002; Giambiagi and Martínez, 2008; Rocher and Vallecillo, 2014). In addition, a series of mainly west-dipping regional normal faults (Fig. 1B) apparently controlled the development and location of large calderas during the Choiyoi volcanism (Llambías and Sato, 1995; Rocher and Vallecillo, 2014), with extension propagating from east to west creating successive depocenters (Malizia et al., 1999; Heredia et al., 2002; Cardó et al., 2005). Likewise, in the study area, the Olivares and Carmen faults (Fig. 2) are thought to have had normal activity during the Permian, accommodating volcanic deposits (Velásquez et al., 2021).

The Triassic part of the pre-Andean stage witnessed the development of NW-SE trending rift basins in the forearc (San Félix; Salazar *et al.*, 2020) and retroarc (Bermejo, Cuyo; Barredo *et al.*, 2012; Sato *et al.*, 2015) areas of SW Gondwana (Fig. 1A). Sedimentation in the San Félix basin, however, would have begun as early as ~255 Ma and extended into the Middle Triassic according to U-Pb ages of detrital zircons (Fig. 1C; Salazar *et al.*, 2020).

A significant deformation event during the pre-Andean stage is the Huárpica extensional phase, represented in Argentina by a regional discordance that separates the Choiyoi Group volcanics from the overlying Late Triassic-Early Jurassic deposits associated with the rift basins (Fig. 1C). The Huárpica phase is thus interpreted as the beginning of the Triassic rifting along crustal weakness zones, inherited from the accretion of allochthonous terranes along the southwestern margin of Gondwana (Charrier et al., 2007; Llambías and Sato, 2011; Sato et al., 2015). On the other hand, in the Frontal Cordillera of Chile, the Permian to Triassic stratigraphic record is marked by three discordances (Fig. 1C). The three deformational events interpreted from these discordances have a more local influence and cannot be directly correlated to the Huárpica phase, mostly because there are no clear equivalents to the Choiyoi Group and Triassic rift basin deposits in Chile. Nevertheless, these discordances have been interpreted as exhumation events developed in an extensional tectonic setting, similar to that of the Huárpica phase in Argentina (Salazar et al., 2020; Velásquez et al., 2021).

Along the Frontal Cordillera, the pre-Andean stage deposits have been affected by thick-skinned deformation linked to Eocene and Miocene compressional events (Moscoso and Mpodozis, 1988; Fosdick *et al.*, 2015; Lossada *et al.*, 2017). Thus, in the study area, these rocks are arranged in structural blocks separated by regional reverse and inverted normal faults (Velásquez *et al.*, 2021) (Fig. 2).

3. Methodology

Three stratigraphic sections were described in the La Laguna sector (Fig. 2), together with the collection of new geological and structural data. This was complemented with data from previous field campaigns of Sernageomin and petrographic descriptions of 50 thin sections. The lithofacies coding used in this work is based on the nomenclature of D'Elia *et al.* (2012) for volcanic rocks, Branney and Kokelaar (2002) for pyroclastic rocks, and Miall (2006) for sedimentary rocks.

The petrographic descriptions were carried out with an Olympus polarizing microscope, model BX51, with a magnification range of 4-40x. The photomicrographs were taken with a 5 MP Micrometrics camera with a CCD sensor, model 590CU. For lavas and pyroclastic rocks, the International Union of Geological Sciences (IUGS) classification scheme (Le Maitre *et al.*, 2002) was used, while for siliciclastic and carbonate rocks, the nomenclature of Folk (1954, 1980) and Dunham (1962) were employed.

4. Stratigraphy and lithofacies analysis

Three stratigraphic sections were described in rocks of the El Tapado and Guanaco Sonso formations: Ingagúas, El Tapado, and Las Tetas (Fig. 3). These

sections are part of different structural blocks, bounded by the Baños del Toro, La Laguna, and Olivares faults (Fig. 2). The Las Tetas and El Tapado sections (modified from Castillo, 2021), placed in the eastern and central blocks respectively, comprise pyroclastic and sedimentary rocks of the El Tapado Formation, whereas the Ingaguás section (modified from Velásquez *et al.*, 2021), placed in the western block, includes dominantly pyroclastic rocks of the Guanaco Sonso Formation.

The lithofacies analysis carried out in this work allowed for the definition of 32 lithofacies: 18 volcanic and 14 sedimentary, whose codes, descriptions, and interpretations are shown in table 1. These lithofacies were grouped into lithofacies associations, from which the depositional environments were inferred, as illustrated in figure 3. Hereunder, the description and interpretation of each lithofacies association is presented. More comprehensive information on this section can be found in Appendix A: Stratigraphy and lithofacies analysis.

4.1. Volcanic lithofacies associations

4.1.1. Mafic volcanism

VM1: Basaltic-andesitic to andesitic lavas (cB, cA) Description: Packages of meter-scale, coherent basaltic-andesitic (cB) to andesitic (cA) lavas (Fig. 4A). The lavas are mostly porphyritic and subordinately aphanitic in texture, with plagioclase and olivine phenocrysts in the case of cB, and plagioclase and subordinate amphibole phenocrysts in the case of cA. Amygdaloidal texture is common in these lavas, particularly in cB, with calcite and zeolite fillings (Fig. 4B). The packages develop columnar jointing and lose lateral continuity after several tens of meters. Interpretation: Subaerial mafic to intermediate lava flows of relatively low volume, probably very close to the emission center. Their amygdaloidal texture indicates significant volatile exsolution (e.g., McPhie et al., 1993).

4.1.2. Intermediate volcanism

VI1: Proximal andesitic volcanism (mBr, mlLT, frmT, cA)

Description: This association groups massive pyroclastic breccias (mBr), lithic-rich massive ash-lapilli tuffs (mlLT), fine-rich massive ash tuffs (frmT), and subordinate andesitic lavas (cA). mBr and mlLT are matrix-supported, poorly to very poorly sorted, and contain mostly polymictic volcanic

Castillo et al. / Andean Geology 52 (1): 1-46, 2025

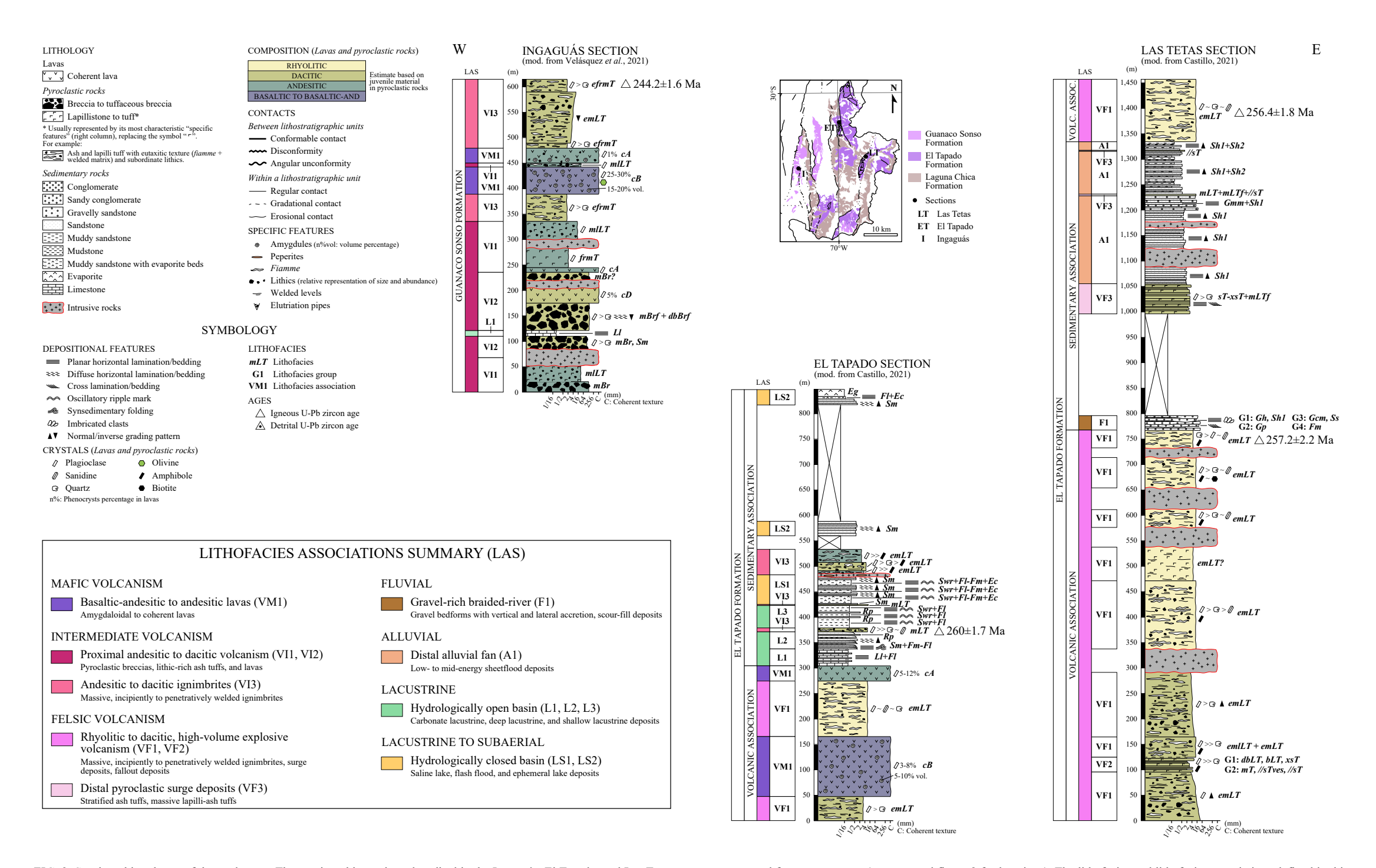


FIG. 3. Stratigraphic scheme of the study area. The stratigraphic sections described in the Ingaguás, El Tapado, and Las Tetas areas are presented from west to east (see map and figure 2 for locations). The lithofacies and lithofacies associations defined in this work are indicated in each section. The Lithofacies Associations Summary (LAS) synthesizes the main volcanic products and sedimentary environments interpreted. The same colors from the LAS are used in the paleoenvironmental scheme of figure 11.

All U-Pb zircon ages are from Velásquez et al. (2021). The legend and symbology in this figure also apply to the rest of the stratigraphic schemes in this work.

TABLE 1. CARACTERIZATION OF THE LITHOFACIES DEFINED IN THIS WORK.

Lithofacies	Lithology	Description	Geometry and thickness	Interpretation	Associations
Volcanic roc	eks				
сВ	Basaltic andesite	Coherent lava. Aphanitic to porphyritic. Sometimes with high amygdule content.	Tabular to lenticular. Meter-scale layers.	Subaerial mafic lava flow.	VM1
cA	Andesite	Coherent lava. Porphyritic to aphanitic. Locally amygdaloidal.	Tabular. 0.5-2 m thick.	Subaerial intermediate lava flow.	VM1; VI1
cD	Dacite	Coherent lava. Massive. Slightly porphyritic.	Tabular. 0.5-3 m thick.	Subaerial felsic lava flow.	VI2
mBr	Breccia to tuffaceous breccia	Massive. Matrix- supported. Very poorly sorted.	Irregular. Erosive to flat base. Decimeter- to meter- scale layers.	High-energy pyroclastic density current deposit. Deposition controlled by fluid escape or granular flow.	VI1; VI2
mBrf	Breccia to tuffaceous breccia	Massive. Matrix- supported, with clast- supported local domains. Poorly sorted. Fabric of clasts elongated parallel to the bedding plane. Commonly with inverse lithic gradation.	Irregular. Erosive to flat base. Decimeter- to meter- scale layers.	High-energy pyroclastic density current deposit. Deposition controlled by fluid escape, but with significant shear near the base of the current and hence a granular flow component.	VI2
dbBrf	Breccia to tuffaceous breccia	Diffusely bedded. Matrix- supported, with clast- supported local domains. Poorly to moderately sorted. Fabric of clasts elongated parallel to the bedding plane. Commonly with inverse lithic gradation.	Irregular. Erosive to flat base. Decimeter- to meter-scale layers.	High-energy pyroclastic density current deposit. Deposition controlled by granular flow, as energy transfer between particles becomes less than frictional forces.	VI2
mLT (e)	Ash-lapilli tuff to lapilli-ash tuff	Massive. Matrix- supported. Poorly to very poorly sorted. Lithic clasts up to 8 cm in diameter. Fiamme up to 12 cm long (when present). With or without eutaxitic texture. Sometimes with normal or inverse lithic gradation.	Tabular. Flat to gradational base. Decimeter- to meterscale layers. Sets of several tens of meters (<150 m in total).	Pyroclastic density current deposit. Deposition controlled by fluid escape, facilitating rapid aggradation.	VI3; VF1; VF3
mlLT (e)	Ash-lapilli tuff	Similar to <i>mLT</i> , but with a high concentration of lithics (>25%vol.).	Tabular to irregular. Erosive flat to irregular base. Few dm thick.	Pyroclastic density current deposit. Deposition controlled by fluid escape, with energy level in between <i>mLT</i> and <i>mBr</i> .	VII; VF1
mLTf(e)	Ash-lapilli tuff to lapilli-ash tuff	Similar to <i>mLT</i> , but with a fabric of clasts elongated parallel to the bedding plane.	Tabular. Flat to gradational base. Centimeter- to decimeter-scale layers.	Pyroclastic density current deposit. Deposition controlled by fluid escape, but with significant shear near the base of the current and hence a granular flow component.	VF3

Table 1 continued.

Lithofacies	Lithology	Description	Geometry and thickness	Interpretation	Associations
dbLT	Ash-lapilli tuff to ash tuff	Diffuse bedding and stratification, defined by gradations (normal or inverse) of fragment size and concentration. Matrixto clast-supported. Poorly to moderately sorted. Relatively low fragment size (generally <1 cm). Fabric of clasts elongated parallel to the bedding plane.	Tabular. Flat to slightly erosive base. Some dm to a few m-thick layers.	Pyroclastic density current deposit. Deposition under conditions intermediate between those dominated by fluid escape and traction in terms of concentration and shear gradients. It records subtle instabilities in the particle concentration or velocity of a current as it deposits.	VF2
bLT	Ash-lapilli tuff to ash tuff	Similar to <i>dbLT</i> , but with abrupt, better defined bedding planes.	Tabular. Centimeter- scale layers.	Analogous to <i>dbLT</i> , but with more abrupt instabilities during deposition.	VF2
frmT (e)	Ash tuff	Massive. Matrix- supported. Poorly sorted, fine-rich and with scarce lithics. Fine to coarse ash size, with very scarce lapilli, May have eutaxitic texture.	Tabular. Flat base. Decimeter-scale layers.	Smaller grain-size equivalent of lithofacies <i>mLT</i> . Low-concentration pyroclastic density current deposit, with aggradation controlled by fluid escape.	VI1; VI3
sT	Ash tuff	Discontinuous horizontal stratification, with occurrence of erosive truncations. Clast-supported. Good to moderate sorting. Coarse ash size.	Tabular to lenticular. Flat, erosive or gradational base. Centimeter- to decimeter-scale layers.	Pyroclastic density current deposit. Deposition dominated by traction processes.	VF3
xsT	Ash tuff	Low angle cross- lamination with low lateral continuity. Clast- supported. Good sorting. Coarse ash size.	Tabular to lenticular. Flat, erosive or gradational base. Centimeter- to decimeter-scale layers. Internal erosive truncations.	Pyroclastic density current deposit. Deposition dominated by traction processes. Current with low aggradation rate, or too unstable to keep a sustained deposition.	VF2; VF3
mT	Ash tuff	Massive. Good sorting. Coarse to fine ash size. Slight vesicular texture (<10%vol.).	Tabular. Flat base. <80 cm-thick layers.	Ash-fall deposit.	VF1; VF2
//sT	Ash tuff	Continuous horizontal stratification. Good sorting. Fine to coarse ash size.	Tabular. Flat base. <20 cm-thick layers.	Ash-fall deposit, or a co- ignimbrite deposit formed by an ash-rich pyroclastic density current.	VF1; VF2; VF3
//sTves	Ash tuff	Discontinuous horizontal stratification. Vesicular texture (25-30%vol.) with ellipsoidal to irregularly shaped vesicles. Moderately sorted.	Tabular. Flat base. <30 cm-thick layers.	Ash-fall in humid conditions (e.g., due to rain, or in the context of a phreatomagmatic eruption).	VF2
Rp	Ash tuff to lapilli-ash tuff	Massive to diffusely laminated. Poorly to moderately sorted. Coarse ash and sparse lapilli.	Tabular. Flat base. <50 cm-thick layers.	Pyroclastic airfall or flow redeposited subaqueously by epiclastic processes.	L2; L3

Table 1 continued.

Lithofacies	Lithology	Description	Geometry and thickness	Interpretation	Associations
Sedimentary	vrocks				
Gem	Conglomerate	Clast-supported. Massive. Moderately sorted.	Lenticular to tabular. Erosive to gradational base. <30 cm-thick layers.	Inertial bedload, deposited by a turbulent pseudo- plastic debris flow.	F1
Gmm	Gravelly sandstone to sandy conglomerate	Matrix-supported. Massive. Poorly sorted. Clasts up to 20 cm in diameter, commonly oriented parallel to the stratification plane.	Tabular to lenticular. Flat to slightly erosive base. 0.2 to 1 m-thick layers.	Hyperconcentrated supercritical flow deposit.	A1
Gh	Conglomerate to gravelly sandstone	Clast- to matrix-supported, with horizontal bedding. Poorly to moderately sorted. Commonly with imbrications.	Tabular. Erosive to flat base. A few dm to a couple of m-thick layers.	Longitudinal bedforms. Bedload deposition in episodes of high water and sediment discharge.	F1
Gp	Conglomerate to gravelly sandstone	Clast- to matrix-supported, with planar crossbedding. Moderately to poorly sorted.	Tabular. Flat to erosive base. A few dm to a couple of m-thick layers.	Transverse bedforms, deltaic growths from remnants of old bars.	Fl
Ss	Conglomerate to gravelly sandstone	Massive or with poorly defined lamination. Poorly to moderately sorted.	Irregular to lenticular. Erosive to gradational base. <20 cm-thick layers.	Scour-pool fill deposits.	F1
Sm	Sandstone to gravelly sandstone	Clast-supported. Massive to diffusely laminated, commonly with normal gradation. Moderate to good sorting (varies to poor, depending on vitroclastic content).	Markedly tabular to irregular. Flat to erosive base. Centimeter- to decimeter-scale layers.	Rapid sedimentation from high-energy flows in waning conditions.	VI2; L2; LS1; LS2
Swr	Sandstone (fine- to medium- grained)	Wave rippled, varying to sinuously laminated or even massive. Good to moderate sorting.	Wavy to lenticular. Erosive base. Millimeter- to centimeter-scale layers.	Tractional sedimentation by oscillatory flows.	L3; LS1
Sh1	Sandstone	Horizontal lamination or bedding, with oriented clasts. Moderate to good sorting. Normal gradation is common.	Tabular. Flat to erosive flat base. Centimeter- to decimeter-scale layers.	Supercritical (relatively high energy and low depth) flow deposit.	F1; A1
Sh2	Sandstone to muddy sandstone	Horizontal lamination, with oriented clasts. Moderate to poor sorting.	Tabular. Flat base. Centimeter- to decimeter-scale layers.	Lower-energy equivalent of <i>Sh1</i> . Supercritical to subcritical flow deposit.	A1
Fl	Mudrock to sandy mudrock	Fine horizontal lamination. Sand is very fine- to fine-grained when present.	Tabular to lenticular. Flat base. Millimeter- to decimeter-scale (<40 cm) layers.	Decanting of fine- suspended sediment in low-energy conditions.	L1; L2; L3; LS1; LS2

Table 1 continued.

Lithofacies	Lithology	Description	Geometry and thickness	Interpretation	Associations
Fm	Mudrock to sandy mudrock	Massive or with loose lamination.	Tabular to lenticular. Flat base. Millimeter- to decimeter-scale (<40 cm) layers.	Decanting of fine- suspended sediment in low-energy conditions.	F1; L2; LS1
Ll	Calcilutite to calcarenite	Fine horizontal lamination.	Tabular. Flat base. Decimeter-scale layers.	Decanting of suspended biogenic calcareous material.	VI2; L1
Ec	Evaporitic calcite	-	Lenticular. Millimeter- to centimeter-scale layers.	Direct precipitation of calcium carbonate.	LS1; LS2
Eg	Evaporitic gypsum	-	Tabular. Centimeter- to meter-scale layers.	Direct precipitation of hydrated calcium sulfate.	LS2

For each volcanic and sedimentary lithofacies, a brief description is presented in terms of its lithology, general features, geometry, and thickness, along with an interpretation derived from those characteristics. The symbol 'e' stands for eutaxitic texture and is added at the beginning of the code of some lithofacies when this feature is present; for example: *emLT*.

lithics and plagioclase crystals in a vitreous matrix. Locally, *mlLT* shows abundant juvenile andesitic lithics with elongated to equidimensional shapes, diffuse to well-defined rounded edges, and variable crystallinity grade (Fig. 4C). *frmT* is matrix-supported and poorly sorted, with an abundant vitreous matrix surrounding mostly plagioclase crystals; while *cA* has a porphyritic texture, with scarce plagioclase phenocrysts.

Interpretation: *mBr* and *mlLT* are proximal (*i.e.*, nearvent) volcanic deposits associated with high-energy pyroclastic density currents, with fluid escape as the dominant depositional control, as suggested by their massive structure and poor sorting (e.g., Branney and Kokelaar, 2002; Sulpizio and Dellino, 2008). The variable shape, texture, and crystallinity grade of the juvenile lithics in *mlLT* suggest differences in magma rheology, which may be associated with magmatic chamber zonation (e.g., Hernando et al., 2019). frmT is interpreted as a smaller grain-size equivalent of *mLT*, formed by low-particle-concentration pyroclastic density currents, depleted in lithics. The intercalation of lavas and high- to low-concentration pyroclastic flow deposits is attributed to variable volatile content in the magmatic source, possibly associated with

cycles of new magma injection. Mineral content suggests overall andesitic compositions.

VI2: Proximal dacitic volcanism (cD, mBr, mBrf, dbBrf, Sm, Ll)

Description: Massive pyroclastic breccias (*mBr*) and massive to diffusely bedded pyroclastic breccias with directional grain fabric (mBrf, dbBrf) of dacitic composition, intercalated with dacitic lavas (cD), massive sandstones (Sm), and redeposited calcilutites (L1). The breccias (mBr, mBrf, dbBrf) are generally poorly sorted and matrix-supported, and form decimeter- to meter-scale layers. Particularly, mBrf and dbBrf develop inverse lithic gradation and have clast-supported domains (Fig. 4D). In the lower part of the Ingaguás section, the breccias are capped by thin levels of calcilutites of tabular to irregular shape, with abrupt thickness variations and partially mixed with the vitreous ash matrix (Fig. 4D). cD lava flows are massive, slightly porphyritic in texture, and have plagioclase phenocrysts. Sm are fine- to medium-grained sandstones, arranged in centimeterto decimeter-scale tabular layers.

Interpretation: The intercalation of pyroclastic breccias and lava flows points to intense degassing of the magmatic source (*e.g.*, Cas and Wright, 1987).

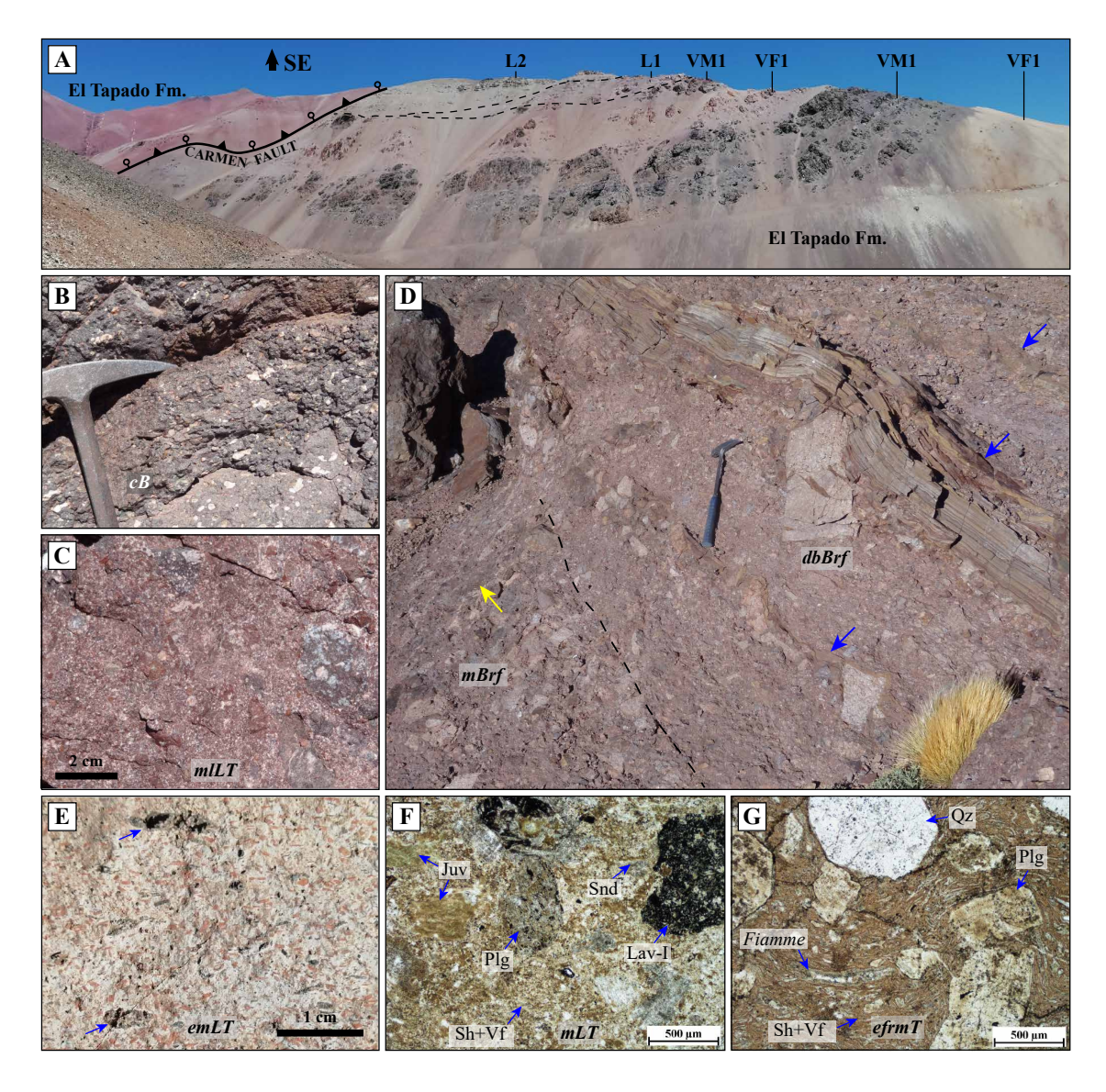


FIG. 4. Mafic and intermediate volcanic lithofacies associations. A. Outcrop in the El Tapado area, showing deposits of associations VM1, VF1, L1, and L2. The dashed lines highlight the lateral wedging of the L1 succession. Towards the east, the Carmen fault contacts the succession with ignimbrites from the same El Tapado Formation. B. Basaltic lavas of VM1 showing amygdules with calcite, zeolite, and clay fillings. C. Massive ash-lapilli tuff of VI1 presenting andesitic juvenile lithics with variable shapes and textures. D. Massive to diffusely stratified tuffaceous breccias of VI2. The layers exhibit inverse grading and are topped by redeposited calcilutites (blue arrows). On the left side of the image (yellow arrow), the fabric of the clasts becomes subvertical due to accommodation around a metric clast (absent). E. Andesitic lapilli-ash tuff of VI3. The matrix has a white clay patina, feldspars are altered to brown clays, and juvenile fragments (arrows) exhibit advanced chloritization. F. PPL photomicrograph of an ignimbrite of VI3. It shows flattened to irregular juvenile vitroclasts (Juv) replaced by chlorite, plagioclase (Plg) and sanidine (Snd) crystals, and an intermediate lava lithic (Lav-I), in an incipiently welded, strongly smectitized matrix of glass shards and vitreous fine ash (Sh+Vf). G. PPL photomicrograph of an ash tuff of VI3. It presents quartz (Qz) and clay-altered plagioclase (Plg) crystals, and small, sparse fiamme in a matrix of glass shards and vitreous fine ash (Sh+Vf) with moderate welding and selective replacement of fine ash by iron oxides. PPL: Plane-polarized light.

The breccia lithofacies suggest variable deposition mechanism controls, from fluid escape (*mBr*) to granular flow (*dbBrf*), with *mBrf* in between (*e.g.*, Branney and Kokelaar, 2002; Sulpizio and Dellino, 2008). These deposits match the model of Sulpizio and Dellino (2008) of stepwise aggradation of successive pulses caused by *en masse* freezing. The redeposited calcilutites would have been removed in a semi-consolidated state by the current and transported at the top of each pulse by buoyancy effects. The intercalated *Sm* layers are interpreted as laharic events, probably hyperconcentrated flows (*e.g.*, Smith and Lowe, 1991). Mineral content suggests overall dacitic compositions.

VI3: Andesitic to dacitic ignimbrites (emLT, mLT, efrmT)

Description: Massive, mostly eutaxitic ash-lapilli to lapilli-ash tuffs (*emLT* and *mLT*) and massive, eutaxitic, fine-rich ash tuffs (*efrmT*), of andesitic to dacitic composition. These lithofacies are poorly to very poorly sorted, and composed of *fiamme*, plagioclase, quartz, and amphibole crystals, and volcanic lithics in a glassy matrix, with incipient to penetrative welding (Fig. 4E to G). In the Ingaguás section, *efrmT* is dominant and *emLT* develops inverse lithic gradation (Fig. 3). In the El Tapado section, only *emLT* and *mLT* are present, forming relatively thin ignimbrites intercalated in a sedimentary succession (Fig. 3).

Interpretation: Explosive intermediate volcanic products, whose welding and massive structure are consistent with deposition controlled by fluid escape from high-temperature pyroclastic density currents (*e.g.*, Branney and Kokelaar, 2002). The smaller grain-size and lithic depletion of the *efrmT* ignimbrites is attributed to a relatively lower particle concentration of the forming current. Particularly, the incipient welding of *mLT*, intercalated between lithofacies associations L2 and L3 (Figs. 3 and 4F), is consistent with hot emplacement in shallow waters (*e.g.*, Cas and Wright, 1991).

4.1.3. Felsic volcanism

VF1: Dacitic to rhyolitic ignimbrites (emLT, emlLT, //sT, mT)

Description: Decimeter- to meter-scale, eutaxitic, massive ash-lapilli to lapilli-ash tuffs (*emLT*), with subordinate layers enriched in lithic fragments (*emlLT*), rhyolitic to dacitic in composition. Locally, thin (cm-thick) layers of parallel-stratified ash

tuffs (//sT) and massive ash tuffs (mT) crown the ignimbrites. In emLT and emlLT, sorting is poor to very poor, comprising fine ash, glass shards and juvenile clasts. Welding is mostly moderate to dense, forming flattened glass shards and fiamme (Fig. 5A to C). Other ignimbrites show incipient welding, with amoeboid to irregular juvenile clasts (Fig. 5D). Lithics consist of angular polymictic volcanic fragments, commonly with irregular or concave shapes and argillaceous halos. They show normal gradation in some deposits of the Las Tetas section (Fig. 3). Crystals are very common and correspond mainly to plagioclase, quartz and sanidine, with subordinate amphibole and biotite (Fig. 3).

Interpretation: The poor sorting and massive structure of these ignimbrites are consistent with a deposition mechanism controlled by fluid escape, which typically operates in currents with concentrated basal parts and leads to rapid particle aggradation (e.g., Branney and Kokelaar, 2002). The large thickness and fine ash content of the deposits is consistent with subcritical pyroclastic flows (sensu Bursik and Woods, 1996), which are relatively slow, thick, and require a high mass flux from the source. The moderate to dense welding is attributed mainly to load compaction during cooling (e.g., Freundt, 1999), although volatile reabsorption, favored by the poor sorting (e.g., Sparks et al., 1999), may have played a significant role as well. The forming currents would have derived from large-volume, low eruption columns (i.e., boiling over) linked to caldera subsidence, in which an instantaneous and continuous collapse of the ejected material occurs (e.g., Branney et al., 1992; Freundt, 1999).

VF2: Phreatomagmatic deposits (dbLT, bLT, xsT, mT, //sT, //sTves)

Description: Succession of ash-lapilli to ash tuffs, dacitic in composition. Two groups of lithofacies are distinguished, which form decimeter- to centimeter-scale intercalations in similar proportions (G1 and G2 in figures 3 and 5E). G1 has a dominance of diffusely bedded ash-lapilli to ash tuffs (dbLT) (Fig. 5I), in some parts with well-defined bedding (bLT), which show a finer grain size compared to ignimbrites from association VF1 (fragments generally <1 cm); locally, there are intercalations of cross-stratified ash tuffs (xsT) (Fig. 5G). G2 includes massive ash tuffs (mT), with minor occurrence of ash tuffs with discontinuous (//sTves) and continuous (//sT) horizontal stratification (Fig. 5F), the former with a conspicuous vesicular

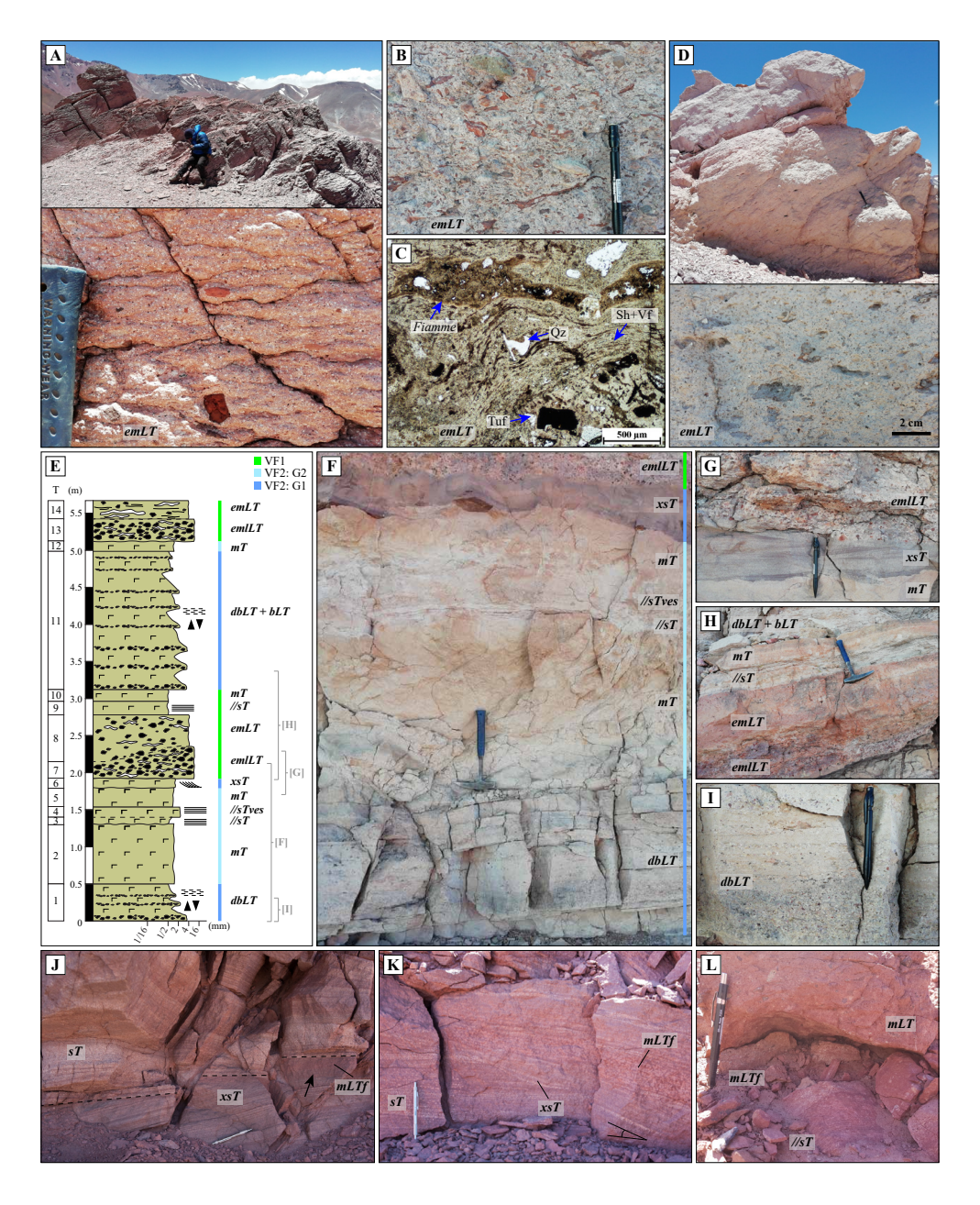


FIG. 5. Felsic volcanic lithofacies associations. A. Rhyolitic, densely welded ignimbrite of VF1 in the middle part of the Las Tetas section. B. Dacitic, densely welded ignimbrite of VF1 at the base of the Las Tetas section. C. PPL photomicrograph of a rhyolitic ignimbrite of VF1 at the top of the Las Tetas section. It has eutaxitic texture, with a matrix of glass shards and vitreous fine ash (Sh+Vf). A *fiamme* altered to iron oxides, an angular tuffaceous lithic clast (Tuf), and an embayed quartz crystal (Qz) are also indicated. D. Rhyolitic ignimbrite of VF1 underlying a fluvial package at the Las Tetas section. It has incipient welding, with amoeboid juvenile vitroclasts. E. Detailed stratigraphic section of the upper part of the VF2 succession, showing its close relation with VF1. Thorough descriptions of the intervals (T) can be found in table A1 in Appendix A. References to photographs within this figure are provided. Symbology as in figure 3. F. Deposits of VF2, indicating intercalation of groups G1 and G2. G. Close-up to lithofacies xsT, showing low-angle cross-lamination (5-15°) and numerous erosive truncations. H. Deposits of VF1 intercalated in the VF2 succession. I. Diffuse bedding of lithofacies dbLT, resulting from normal and inverse gradations in clast size and proportion. J. Stratified ignimbrite of VF3, showing erosive (dashed line) to gradational (arrow) contacts between lithofacies. K. Close-up to ignimbrite of VF3, highlighting an angular erosive base of xsT and the oriented fabric of mLTf. L. Pyroclastic deposits of VF3 intercalated in the alluvial succession of the Las Tetas section. PPL: Plane-polarized light.

texture and all with a typically good sorting. This association has intercalated deposits of VF1, as shown in figure 5H and E presents a detailed segment from the lower part of the Las Tetas section, showing the interplay between deposits of VF2 and VF1. A thorough description of this section is presented in table A1 in Appendix A.

Interpretation: The deposits of G1 are consistent with base surge deposits (e.g., Cas and Wright, 1987), formed by cold and highly mobile currents related to phreatomagmatic activity (e.g., Self, 1983; McPhie, 1986). These currents typically have concentrated, granular flow-dominated basal parts, with unsteady deposition due to turbulence (e.g., Branney and Kokelaar, 2002). On the other hand, deposits of G2 indicate direct fallout-dominated deposition (e.g., Talbot et al., 1994), partly in the presence of liquid water, which favors the entrapment of air bubbles (e.g., Walker, 1971, 1981). Altogether, the association is interpreted as phreatomagmatic deposits given the intercalations of base surge and ash fall deposits (e.g., Self, 1983; McPhie, 1986; Branney, 1991). The intercalations of VF1 in VF2 in the Las Tetas section are thought to reflect an episodic decrease in water influence on the eruption mechanism (Self, 1983).

VF3: Distal pyroclastic surge deposits (sT, xsT, mLT, mLTf, //sT) Description: This association groups thin (<dm-

thick) stratified pyroclastic deposits intercalated in the Las Tetas section (Fig. 3). The main package consists of interbedded layers of stratified (sT) and cross-stratified (xsT) ash tuffs, and massive lapilli-ash tuffs with directional grain fabric (*mLTf*). The layers show flat erosive to gradational bases (Fig. 5J and K). sT and xsT are dominantly crystalline, clast-supported, and moderately to well sorted. In turn, *mLTf* is dominantly vitric, matrix-supported, and poorly sorted, with its fabric defined by abundant vitreous juvenile pyroclasts (Fig. 5K). Other deposits intercalated consist of a thin succession of mLT, mLTf, and //sT (Fig. 5L), and an isolated deposit of //sT. **Interpretation:** The overall dominance of traction deposition, moderate to good sorting, and high proportion of crystals and lithics of these deposits are consistent with deposition from dilute pyroclastic density currents (i.e., pyroclastic surges) (e.g., Cas and Wright, 1987; Branney and Kokelaar, 2002). The low thickness and grain size of the packages suggest deposition distal from the vent. The main package is associated with a highly turbulent current capable

of depositing and locally eroding. This turbulence would have caused density stratification in the lower (basal) part of the current, segregating the vitric and crystalline material, which followed different depositional mechanisms (traction-dominated for crystal-rich sT-xsT and fluid escape-dominated for vitric-rich mLTf) (e.g., Branney and Kokelaar, 2002). As for the other deposits, the mLT+mLTf+//sT lithofacies group denotes a progressive decrease in particle concentration in the lower part of the forming current (e.g., Branney and Kokelaar, 2002), whereas //sT is indicative of ash-cloud surges (sensu Cas and Wright, 1987), representing the final reaches of the current.

4.2. Sedimentary lithofacies associations

4.2.1. Fluvial

F1: Gravel-rich braided river (Gh, Gp, Gcm, Sh1, Ss, Fm)

Description: Succession of conglomerates, gravelly sandstones, sandstones, and mudrocks, forming meter- to centimeter-scale layers. Its architecture is strongly controlled by different types of contact surfaces, as shown in figure 6A. Four groups of lithofacies are distinguished. G1: horizontally bedded conglomerates to gravelly sandstones (Gh), commonly with imbrications, and locally with thin (cm-thick) intercalations of laminated sandstones (Sh1) (Fig. 6B); G2: conglomerates to gravelly sandstones with planar cross-bedding (Gp) (Fig. 6B to D), commonly showing lateral truncations (Fig. 6A); G3: massive, clast-supported conglomerates (Gcm) intergraded with massive to diffusely laminated, poorly sorted sandstones (Ss) (Fig. 6C and D); and G4: massive mudrocks to sandy mudrocks (Fm) (Fig. 6C).

Interpretation: The horizontally bedded rocks of G1 are associated with deposition as bedload in episodes of high water and sediment discharge, with vertical and frontal accretion, whereas the cross-bedded G2 likely formed by lateral accretion on gravel bar margins (*e.g.*, Smith, 1990; Miall, 2006). The massive conglomerates and sandstones of G3 are interpreted as bedload sedimented rapidly as scour-pool fills (*e.g.*, Ashmore, 1982; Thompson, 1986; Miall, 2006). Finally, the mudrocks and sandy mudrocks of G4 could have decanted from shallow waters with gentle currents (*e.g.*, Smith, 1990), or in ponded waters in abandoned channels (*e.g.*, Miall, 2006). This association is therefore interpreted as

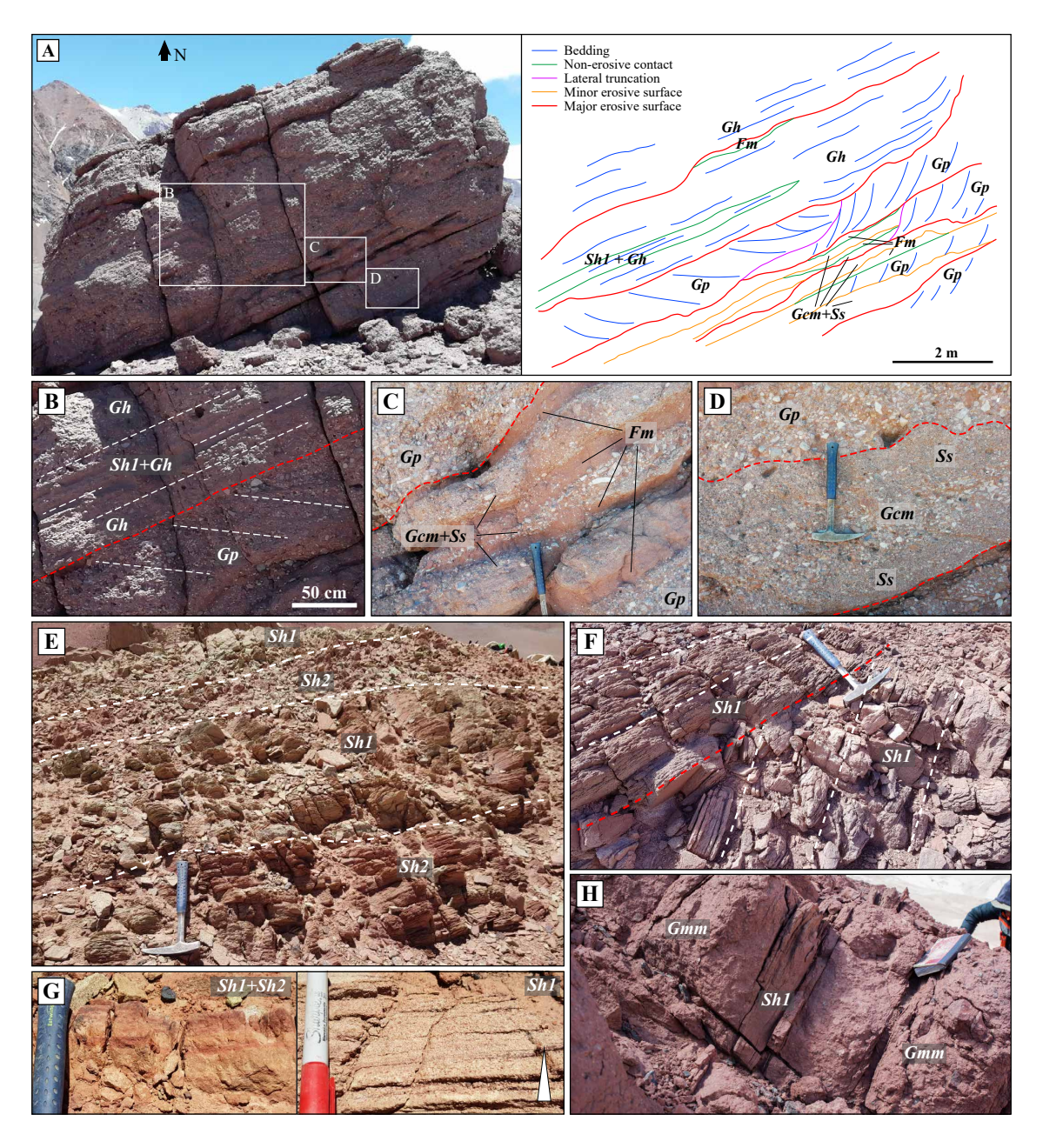


FIG. 6. Fluvial and alluvial lithofacies associations. **A.** Architectural scheme of an outcrop of association F1. Lithofacies and types of contact surfaces are indicated in the right image. The boxes refer to other photographs within the figure. **B.** Horizontally bedded and planar cross-bedded conglomerates and gravelly sandstones of groups G1 and G2, respectively, separated by an erosive surface (red line). **C.** Thin deposits of clast-supported gravels and poorly sorted sands (G3), intercalated with thin layers of massive mudrock (G4). **D.** Deposit of poorly sorted sands and clast-supported gravels (G3) limited by erosive surfaces. **E.** Sets of intercalations of laminated sandstones (*Sh1*) and muddy sandstones (*Sh2*) of association A1. The dominant lithofacies in each set is indicated. **F.** Sets of laminated sandstones of A1 separated by an angular flat erosive surface. **G.** Close-ups of *Sh1* and *Sh2*. The left image shows the color difference between *Sh1* (greenish) and *Sh2* (reddish), which is due to dominant alteration to epidote and iron oxides, respectively. The right image shows normal gradation in *Sh1*. **H.** Massive gravelly sandstones (*Gmm*) of A1, intercalated with laminated sandstones (*Sh1*).

fluvial deposits sedimented in a braided river, with successive cycles of erosion and sedimentation related to flooding pulses followed by waning flow stages (e.g., Smith, 1990; Miall, 2006). These features are consistent with the middle to distal parts of a gravel-dominated braided river (e.g., Hein and Walker, 1977).

4.2.2. Alluvial

A1: Distal alluvial fan (Sh1, Sh2, Gmm)

Description: Redbed succession comprising sets of interbedded, horizontally laminated sandstones and muddy sandstones (*Sh1* and *Sh2*), with intercalated layers of massive gravelly sandstones (*Gmm*) (Fig. 3). *Sh1* and *Sh2* form decimeter- to meter-scale sets in which one lithofacies is dominant over the other (Fig. 6E). The sets are separated by flat to erosive, usually angular surfaces (Fig. 6F). The layers are centimeter- to decimeter-thick, markedly tabular, and *Sh1* commonly develops normal gradation (Fig. 6G). In turn, *Gmm* forms decimeter-thick, tabular to lenticular layers, and contains clasts of up to 20 cm long, oriented parallel to the stratification plane (Fig. 6H).

Interpretation: Sedimentation from unconfined flows or sheetfloods in the distal portion of an alluvial fan, or in an alluvial plain, linked to catastrophic sediment-laden flooding (e.g., Blair and McPherson, 1994; Collinson, 1996; Nichols, 2009). Sh1 and Sh2 deposits are consistent with supercritical flows with reduced competence due to a lower slope in the marginal zone of an alluvial fan (e.g., Blair and McPherson, 1994), whereas Gmm could have been deposited by hyper-concentrated sheetfloods (e.g., Collinson, 1996).

4.2.3. Lacustrine

L1: Carbonate lacustrine (Ll, Fl)

Description: Decimeter-scale deposits of calcilutites and subordinate calcarenites with fine horizontal lamination (Ll) (Fig. 7A and B). In the El Tapado section, centimeter-scale layers of laminated mudrocks to fine-grained sandy mudrocks (Fl) are intercalated (Fig. 7A). Under the microscope, it is observed that Ll is dominantly composed of micrite-rich laminae, along with skeletal fragments, pellets, sand-sized lithics and crystals, and volcanic glass shards, with variable proportions between laminae (Fig. 7C and D). Within the skeletal fragments, remains of very small (<500 μm) and thin concave shells are recognizable (Fig. 7E and F).

Interpretation: Deposition in a carbonate lacustrine environment, with decantation of suspended biogenic calcareous debris from a relatively shallow body of water under low-energy conditions (e.g., Talbot and Allen, 1996). Low-energy siliciclastic inputs were infrequent enough to allow carbonate sedimentation to prevail (e.g., Nichols, 2009) and enabled the preservation of glass shards, indicative of contemporary volcanic activity. The size, shape and thickness of the skeletal fragments suggest they correspond to freshwater organisms, probably branchiopods or ostracods, which are common in shallow continental lacustrine basins (e.g., Gallego and Breitkreuz, 1994).

L2: Deep lacustrine volcaniclastic (Sm, Fm, Fl, Rp) Description: Rhythmic centimeter- to decimeter-scale intercalations between massive to diffusely laminated sandstones (Sm) and laminated to massive mudrocks (Fl and Fm) rich in volcanic clasts (Fig. 8A). Sm has flat, conformable to erosive bases, and commonly displays normal gradation (Fig. 8B). Small synsedimentary folds develop in some rhythmic layers (Fig. 8C). Locally, intercalations of laminated redeposited pyroclastic deposits (Rp) are present (Fig. 8D).

Interpretation: Sedimentation by turbidity currents in a deep lacustrine environment, with deposition of sands as bedload and fines from the trailing cloud (e.g., Cas and Wright, 1987; Nichols, 2009). Synsedimentary folds are attributable to slumping effects, which are common in turbiditic environments (e.g., Elliott and Williams, 1988). The texture and composition of fragments (see Appendix A) suggest a relatively short transport prior to lake entry. The redeposited pyroclastic deposits imply contemporaneous volcanic activity nearby.

L3: Shallow lacustrine volcaniclastic (Swr, Fl, Rp) Description: Millimeter- to centimeter-scale intercalations of laminated mudrocks (Fl) and finegrained sandstones with wave ripples to sinuous lamination (Swr) (Fig. 8E), which develop wavy bedding and flaser bedding (Fig. 8F and G). The mudrocks show mottled colors in shades of green, red, and yellow. Locally, redeposited pyroclastic deposits (Rp) with faint lamination are intercalated (Fig. 8G).

Interpretation: Alternating tractional transport by oscillatory flows and mud settling from suspension, which can be associated with a shallow lacustrine environment (*e.g.*, Rajchl *et al.*, 2008; Nichols, 2009; Melchor *et al.*, 2012). Mottling of mud is attributable

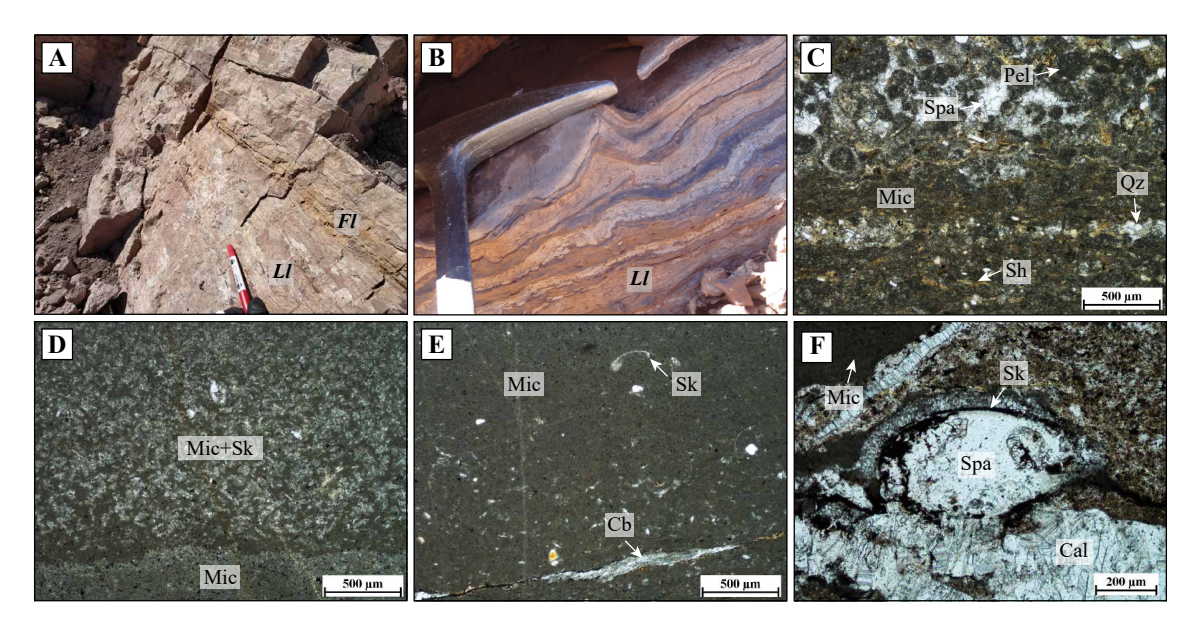


FIG. 7. Carbonate lacustrine lithofacies association (L1). A. Laminated calcilutites and calcarenites (*Ll*) with an intercalated fine-grained sandstone level (*Fl*), in the El Tapado section. B. Close-up of the laminated calcilutites in the Ingaguás section. C. PPL photomicrograph of a sample from the El Tapado section. It shows laminae rich in micrite (Mic), quartz (Qz) and glass shards (Sh), next to a framework of pellets (Pel) and sparite (Spa). D. PPL photomicrograph of a sample from the Ingaguás section (also figure E and F). It displays a lamina enriched in skeletal fragments (Sk) beside a micrite-dominated (Mic) lamina. E. Abundant micrite and scattered skeletal fragments, cut by a carbonate vein (Cb). The labeled skeletal is a thin valve that preserves a relic of its articulation area with the missing valve. F. Thin shell replaced by iron oxides and filled with sparite (Spa). The upper valve is surrounded by another sparite filling, crystallized perpendicular to it. The sample is cut by calcite veins (Cal). PPL: Plane-polarized light.

to pedogenic processes, common in this type of environment (*e.g.*, Tucker, 2003). The redeposited pyroclastic deposits denote contemporaneous volcanic activity nearby.

4.2.4. Saline lacustrine to subaerial LS1: Saline lacustrine volcaniclastic with occasional sheet floods (Swr, Fl, Fm, Ec, Sm)

Description: Succession dominated by sets of thinly (<dm-thick) bedded laminated to massive mudrocks to sandy mudrocks (*Fl* and *Fm*), wave-rippled to sinuously laminated sandstones (*Swr*), and evaporitic calcite (*Ec*), in which meter-scale packages of massive sandstones are interbedded (*Sm*) (Fig. 9A). The detritic-evaporitic sets commonly develop wavy bedding and lenticular bedding, and the mudrocks are laminated (Fig. 9B). In other sectors, these sets show cut-and-fill structures and the mudrocks are massive (Fig. 9B). *Sm* forms centimeter- to decimeter-scale, markedly tabular layers of moderately sorted, very coarse- to fine-grained sand, commonly with normal gradation (Fig. 9C).

Interpretation: Fl, Swr, and Ec are associated with shallow lacustrine sedimentation in a saline lake environment. The evaporites indicate an arid or semi-arid climate and a hydrologically closed basin (e.g., Eugster and Hardie, 1978). Evaporite production would have been controlled by the frequency of clastic inputs into the lake (e.g., Hardie et al., 1978; Nichols, 2009). The Sm packages are attributed to tractional deposition by waning pulses, from unconfined high-energy flows such as flash floods of fluvial or alluvial origin, occurring during subaerial exposure stages (e.g., Benvenut, 2003).

LS2: Sheet floods and ephemeral lakes (Sm, Fl, Ec, Eg)

Description: Packages of decimeter-scale massive sandstones (Sm), intercalated in the upper part of the succession with decimeter-thick packages of laminated mudrocks to sandy mudrocks (Fl) with evaporitic calcite (Ec) lenses, culminating with a meter-scale package of gypsum (Eg). Sm deposits have tabular geometry, moderate to poor sorting, and normal gradation pulses that define a diffuse

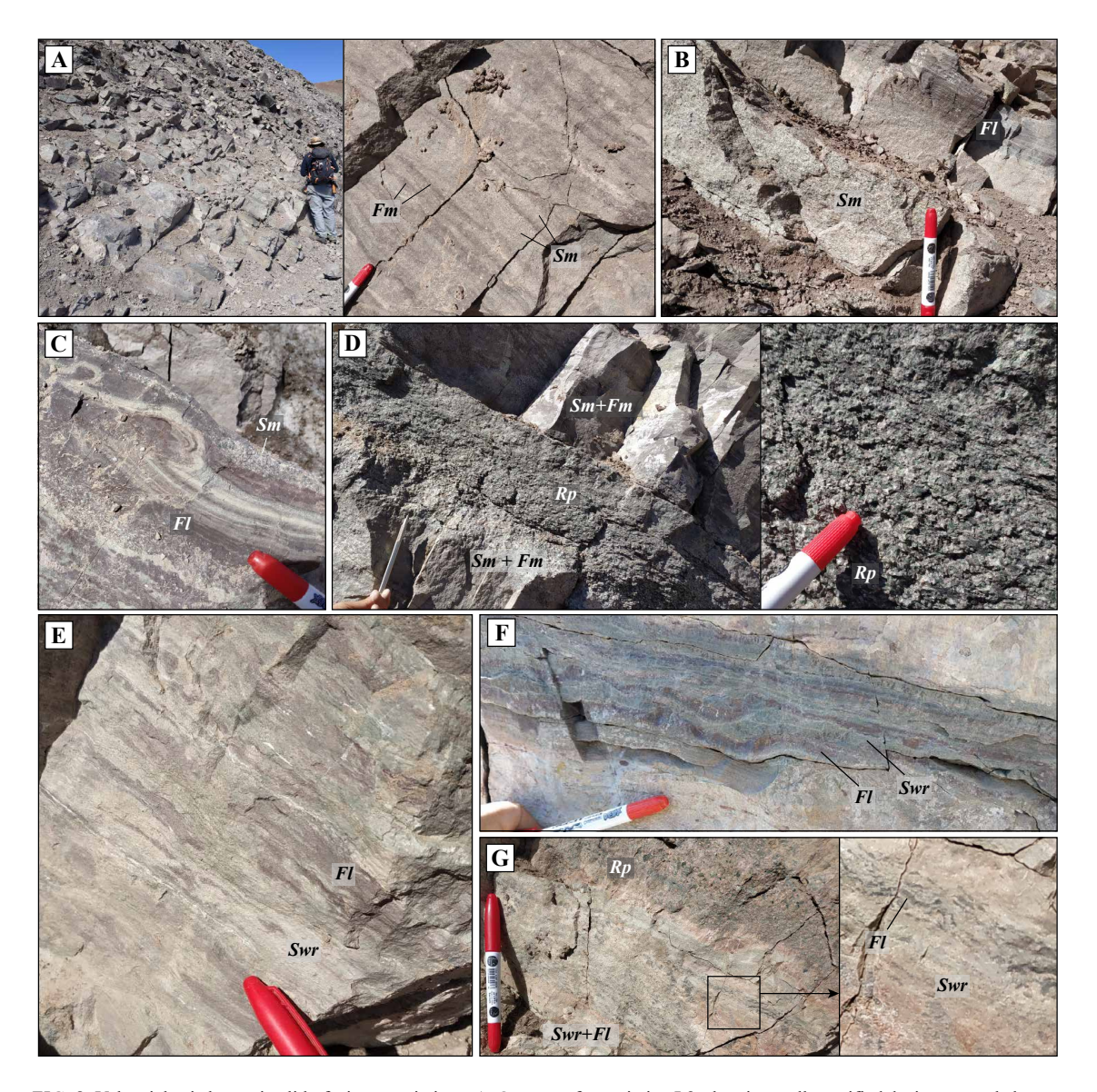


FIG. 8. Volcaniclastic lacustrine lithofacies associations. A. Outcrop of association L2, showing well-stratified decimeter-scale layers. The close-up shows the intercalation of thin levels of massive sandstones and massive mudrocks. B. Layer of sandstone with normal grading from fine gravel to fine sand, covered by a laminated mudrock layer. C. Centimeter-scale synsedimentary folds in L2. D. Redeposited pyroclastic deposit in L2. The close-up shows the preservation of juvenile vitroclasts and coarse glass shards (chloritized), as well as euhedral plagioclase crystals. E. Millimeter-scale intercalations between fine-grained sandstones with wave ripples and laminated mudrocks of association L3. The latter exhibits mottled reddish to yellowish colors. F. Wavy bedding between sandy and muddy layers of L3. G. Deposit of interlaminated sand and mud covered by a redeposited pyroclastic deposit. The close-up shows the formation of flaser bedding in the mudrock.

lamination (Fig. 9D and G). In the Fl and Ec deposits, Fl forms millimeter- to centimeter-thick layers and Ec intercalates as lenses, also millimeter- to centimeter-thick (Fig. 9H). Figure 9E and F show an outcrop and a detail section of these deposits, respectively, in the uppermost 30 m of the El Tapado section.

Interpretation: As in LS1, *Sm* packages would have been formed by unconfined, high-energy flash floods (*e.g.*, Benvenuti, 2003). *Fl* and *Ec* deposits would be the product of sedimentation in ephemeral lakes, with repeated cycles of flooding and evaporation (*e.g.*, Hardie *et al.*, 1978; Lowenstein and Hardie, 1985).

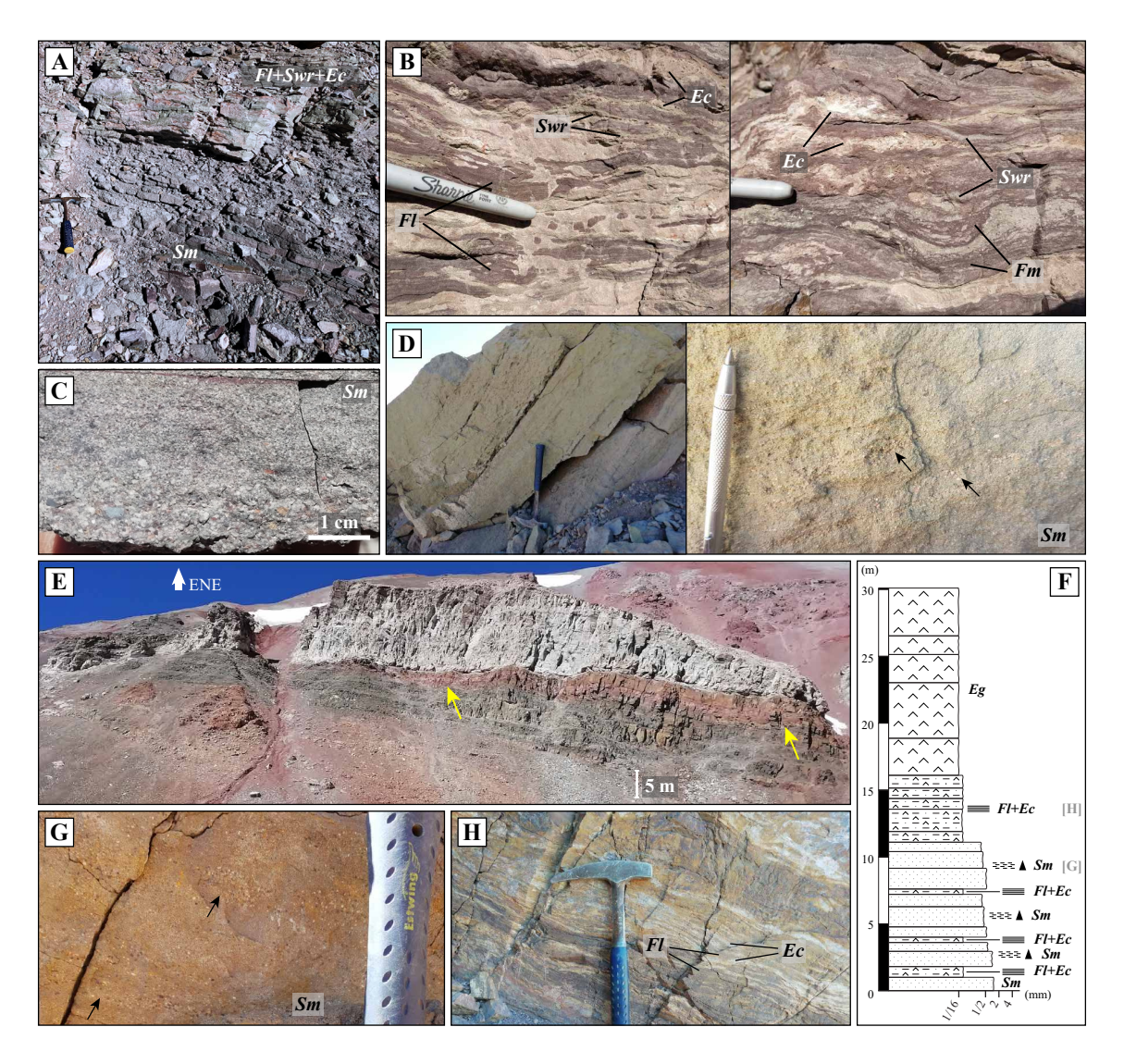


FIG. 9. Lacustrine to subaerial lithofacies associations. **A.** Outcrop of association LS1 showing massive sandstone deposits (*Sm*) overlain by a set of interbedded sandstones, mudrocks and evaporites. **B.** Comparison between *Fl*, *Swr*, and *Ec* deposits. Left: lenticular bedding between laminated mudrocks (*Fl*) and wave-rippled sandstones (*Swr*). Right: Cut-and-fill structures, massive mudrocks (*Fm*). **C.** Close-up of *Sm* showing normal grading from very coarse- to fine-grained sand. **D.** Outcrop of *Sm* deposits of association LS2 in the upper part of the El Tapado section. The close-up shows millimeter-scale levels of very coarse sand to fine gravel deposits (arrows) normally graded towards a domain of medium-sized sand, defining a diffuse horizontal lamination. **E.** Outcrop of the uppermost 30 m of the El Tapado section, consisting of sandstones, mudrocks, and evaporites of association LS2. Arrows indicate the base of a package of *Fl* and *Ec* layers with lateral wedging. **F.** Stratigraphic scheme of the succession of figure 9E, showing a fining-upward trend. The corresponding lithofacies are indicated, along with references to further images within this figure. **G.** *Sm* deposits, showing the same structures as in figure 9D. **H.** Interbedded mudrock to sandy mudrock layers (*Fl*) and evaporitic calcite lenses (*Ec*).

Flash flood and ephemeral lake deposits are a characteristic association of arid depositional environments (e.g., Nichols, 2009). The Eg package

that crowns the section denotes advanced chemical sedimentation, leading to the precipitation of more soluble minerals.

5. Paleoenvironments and stratigraphic relations

5.1. El Tapado Formation

5.1.1. Paleoenvironment

Within the study area, the thickness of the El Tapado Formation reaches its maximum at around 1,500 m in the hanging wall of the Olivares fault in the Las Tetas area (see Las Tetas section in figure 3), and then decreases significantly in the footwall of this structure, where it can reach up to 500 m in thickness and the underlying Laguna Chica Formation is more broadly exposed (Fig. 10A). Based on Velásquez *et al.* (2021), in the northern part of the study area, in the hanging wall between the Carmen and Mercedes faults (Fig. 10B), the thickness of the volcanic rocks varies between 500 and 800 m, which is considerably greater than the thickness observed in the footwall of

the Carmen fault, where the lower volcanic section is <300 m. The thickness of the sedimentary, mostly lacustrine successions is very similar in both structural blocks (see correlation between the El Tapado and Río Seco sections in Section 5.3). The Mercedes fault separates the lacustrine (hanging wall) and pyroclastic (footwall) successions of the El Tapado Formation, the former showing a roll-over geometry, which can be interpreted as a result of synextensional deposition (Fig. 10C). In addition, this fault is partially covered by pyroclastic rocks also assigned to the El Tapado Formation, which constrains the normal faulting within the depositional time span of this unit. It is also relevant to notice that in the western domain of the study area, near the Ingaguás section (Fig. 2), the El Tapado Formation is absent and the Laguna Chica Formation is unconformably overlain by the Guanaco Sonso Formation. Considering the



FIG. 10. Structural observations associated to an extensional setting during the Permian. A. Olivares fault (inverted normal) separating rocks of the Laguna Chica and El Tapado formations in the eastern part of the study area. The beds in the hanging wall have a steeper dip approaching the fault. B. Carmen fault (inverted normal) separating the Laguna Chica and El Tapado formations in the northern part of the study area. The rocks of the El Tapado Formation are also in the hanging wall of the Mercedes fault. This fault is shown in detail in the next figure. C. Mercedes fault (normal) with a roll-over geometry, separating rocks within the El Tapado Formation in the northern limit of the study area. Overlying pyroclastic rocks of the El Tapado Formation are unaltered by the fault, constraining their activity to the Permian.

above, it is inferred that the Olivares, Carmen, and Mercedes faults had extensional activity during the Permian, generating space through tectonic subsidence to accommodate the volcanic and sedimentary deposits of the El Tapado Formation (see figure 11 for a paleoenvironmental evolution scheme). This interpretation is consistent with the Permian west-dipping normal faults described in Argentina to the east of the study area (see Section 2), which are also represented in figure 11.

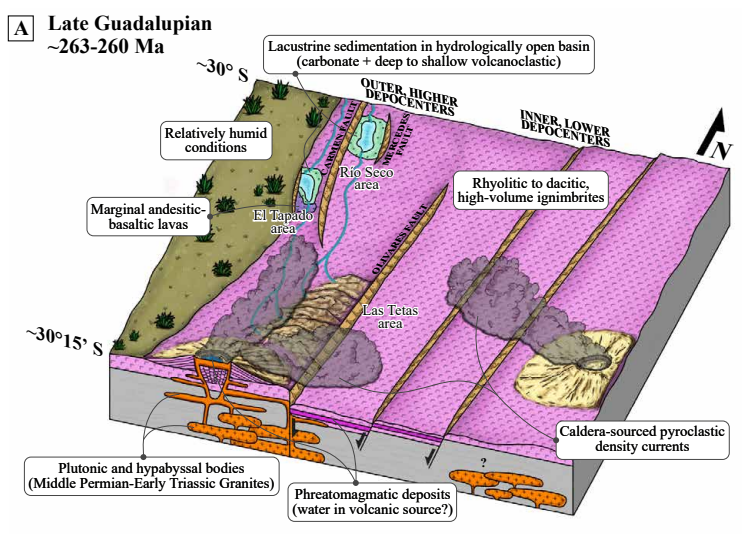
As detailed in Section 4, the thick rhyolitic to dacitic welded ignimbrites of association VF1 are inferred to have been formed by pyroclastic density currents of high mass flow and temperature, derived from low eruption columns linked to caldera subsidence (e.g., Branney et al., 1992; Freundt, 1999; Branney and Kokelaar, 2002) (Fig. 11). The local phreatomagmatic activity recorded in the Las Tetas area (association VF2) is consistent with caldera-forming eruptions as well, as these commonly harbor crater lakes that can come into contact with rising magma and generate this type of activity (e.g., Self and Sparks, 1978; McPhie, 1986). In the El Tapado area, the andesiticdacitic ignimbrites of association VI3 indicate eruptive episodes of lower volume and explosivity that those of association VF1 (Fig. 11B). Thus, the volcanic products of the El Tapado Formation are consistent with a depositional environment dominated by intermediate to felsic volcanic centers, typical of extensional settings (e.g., Cas and Wright, 1987).

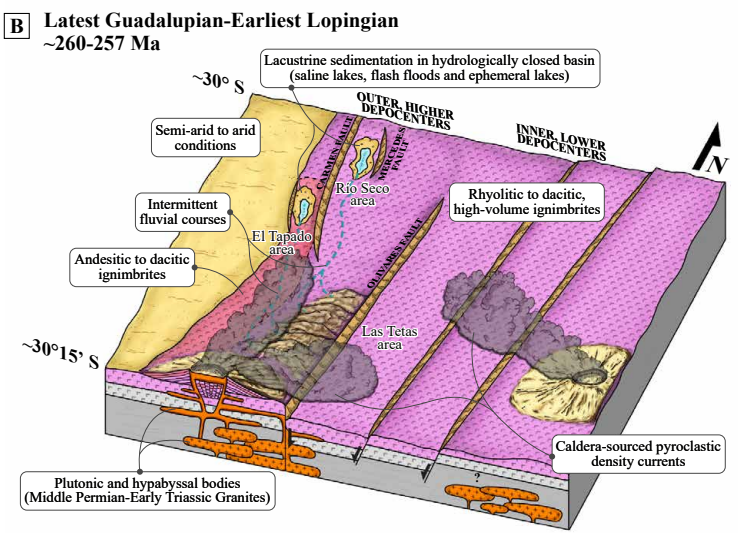
In the Las Tetas area, ignimbrites of VF1 accumulate in thick packages that extend over several kilometers, which points to aggradation over a relatively flat and extensive paleosurface (Fig. 11A and B). These ignimbrites are abundant around rhyolitic centers and can extend for tens of kilometers (*e.g.*, Cas and Wright, 1987), especially if the forming currents were of subcritical type (*e.g.*, Bursik and Woods, 1996). This configuration was also observed in the Upper Choiyoi Group along the Frontal Cordillera,

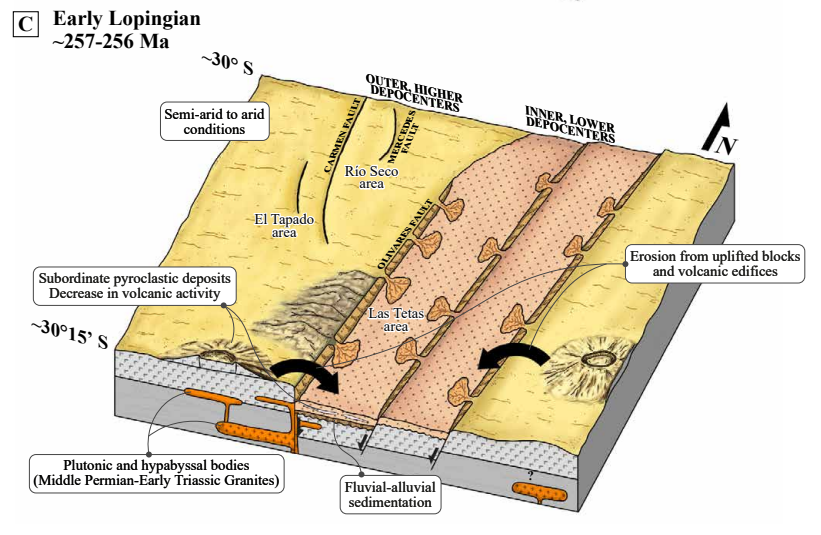
in Argentina, where the superposition of thick and continuous pyroclastic beds derived from different eruptive centers formed extensive ignimbritic plateaus (Llambías et al., 1993). The absence of dacitic to rhyolitic proximal deposits (e.g., breccias, lava domes) in the Las Tetas and El Tapado areas, together with a decrease in the ignimbrite thickness towards the El Tapado area, suggests a medium to distal volcanic environment for these zones relative to the emission centers. A potential indicative of emission center locations can be their coeval plutonic and subvolcanic equivalents. The Colorado river valley hosts acid plutons and hypabyssal rocks of Middle Permian-Early Triassic age (Fig. 2), which are interpreted here to represent the roots of a Permian volcanic system (Fig. 11). These intrusive rocks were emplaced along the trace of the Olivares fault, suggesting that their ascent was facilitated by this structure. In addition, to the east of the study area, a ~20 km-wide band of rhyolitic lavas and ignimbrites of the Choiyoi Group crops out (Malizia et al., 1999), of which the Pata del Indio hill, located southeast of the Agua Negra pass (see figure 1 for locations), is considered an emission center made up of caldera-fill deposits (Sato and Llambías, 1993). This aspect is also represented in figure 11.

The basaltic-andesitic lavas in the El Tapado area (association VM1) are interpreted as marginal products of the rhyolitic volcanism responsible for the ignimbrites (Fig. 11A), since mafic magmas, when they reach the surface, commonly do so outside the rhyolitic center, which acts as a shadow zone (e.g., Cas and Wright, 1987). This mafic activity probably took place along extensional structures acting as eruptive fissures (e.g., Mazzarini et al., 2008). In Argentina, subordinate mafic lavas form part of the Choiyoi volcanic products (Bastías-Mercado et al., 2020), being also common as associated products in other silicic large igneous provinces (e.g., Pankhurst et al., 1998; Bryan et al., 2000; Huang et al., 2016).

FIG. 11. Paleoenvironmental scheme of the El Tapado Formation during the Late Guadalupian-Lopingian. The scheme is contextualized within a rhyolitic volcanic center, with an inner accommodation zone (Las Tetas area) and a more marginal one (El Tapado area) relative to the Late Permian volcanic arc axis. The Río Seco area is also included, following the correlation with the El Tapado section (see Section 5.3). Three evolutionary stages are proposed, constrained based on U-Pb zircon ages reported in the study area by Velásquez *et al.* (2021). The main processes and deposits are labeled in each stage, with the latter represented using the same colors as in the "Lithofacies Associations Summary" from figure 3. Referential eruptive sources are included based on the evidence presented in Section 5.1. A. ~263-260 Ma. Accumulation of volcanic deposits in the Las Tetas and El Tapado areas, and lacustrine sedimentation under relatively humid conditions in the latter. B. ~260-257 Ma. Accumulation of volcanic deposits in the Las Tetas area, and predominance of lacustrine sedimentation under semi-arid to arid conditions in the El Tapado area. C. ~257-256 Ma. Fluvio-alluvial sedimentation in the Las Tetas area. No sedimentation is recorded in the El Tapado area.







In the Las Tetas area, the successive accumulation of thick ignimbrites without sedimentary intercalations suggests that the pyroclastic aggradation rate was much higher than the sedimentation rate, which is consistent with an inner, lower depocenter within an intra-arc environment (Fig. 11). The only exception is the sediment-dominated stage denoted by the fluvial-alluvial succession (associations F1 and A1) intercalated in the upper part of the Las Tetas section. The characteristics of this package are typical of post-eruptive successions, with sediments from reworked volcanic deposits (e.g., Cas and Wright, 1987). Sedimentation likely occurred through alluvial fan systems from uplifted blocks, given the prevalent extensional setting (Fig. 11C). The dominance of sedimentation in this stage is attributed to a transient decrease in volcanic activity, as suggested by the occasional pyroclastic intercalations of association VF3 within the sedimentary succession. In the case of the El Tapado area, the prevalence of lacustrine to subaerial sedimentation is thought to be related to its position in the footwall of the Carmen fault, which would have been a higher and more marginal (i.e., more protected) depocenter with respect to the inferred active emission centers (Fig. 11). In this sense, volcanism would have been active throughout sedimentation in the El Tapado area, as suggested by the occurrence of redeposited pyroclastics in associations L2 and L3, and fallout glass shards in carbonate deposits of L1. In conclusion, the infill of the Las Tetas and El Tapado depocenters was mainly controlled by the rate of volcaniclastic input, together with subsidence dynamics. This relation has also been observed in similar volcaniclastic basins elsewhere (e.g., D'Elia et al., 2016; Espinoza et al., 2019).

5.1.2. Paleoclimate

The sedimentary record of the El Tapado Formation provides very important insights into the paleoclimatic evolution of the Permian in southwestern Gondwana. The El Tapado area hosts carbonate and deep-to-shallow lacustrine deposits (associations L1 to L3), followed by saline lacustrine and flash flood deposits topped by thick evaporite layers (associations LS1 and LS2). This points to a paleoenvironmental evolution from a hydrologically open basin to a hydrologically closed basin, which can be linked to the transition from relatively humid to semi-arid or even arid conditions (*e.g.*, Talbot and Allen, 1996) (Figs. 3, 11A-B). In the Las Tetas area, the fluvial

conglomerates and sandstones of association F1 are followed by ~300 m of alluvial sandstone redbeds of association A1. The switch from a braided river system to an alluvial setting dominated by flash flood events is indicative of increasing aridity (e.g., Owen et al., 1997). Considering this evidence, the El Tapado Formation was likely deposited under an increasingly drier climate, establishing semi-arid conditions from around 260 Ma (Figs. 3 and 11). It must be considered, however, that this is a particular basin, so it cannot be ruled out that the observed water shortage may have been controlled by tectonic activity instead of regional climate changes, affecting the filling and interconnection of highly accommodative basins (e.g., Carroll and Bohacs, 1999). Basin filling also offers an alternative explanation for the shallowing of the environment, up to the establishment of subaerial conditions, although it does not fully explain the observed chemical sedimentation.

Despite these alternatives, an important argument in favor of the climate-driven paleogeographic evolution of the study area corresponds to the observation of similar evidence on a continental scale. In this sense, Limarino et al. (2014) proposed, based on multiple stratigraphic evidence, a four-stage paleoclimatic evolution for the Late Paleozoic of southwestern Gondwana, from a glacial (icehouse) stage in the Late Mississippian to the establishment of semi-arid to arid (greenhouse) conditions in the Late Guadalupian-Lopingian. Within this last stage, observations in the Paganzo retroarc basin in Argentina and the Paraná intraplate basin in Brazil show very similar stratigraphic and paleoenvironmental patterns when compared to the coeval El Tapado intra-arc basin in Chile, as summarized in table 2. Thus, the findings presented in this paper are consistent with the Guadalupian-Lopingian semi-arid to arid stage proposed by Limarino et al. (2014) and constitute the first paleoclimatic evidence in Chilean territory for this period. These findings in southern South America are framed in a series of global environmental changes that occurred during the late Permian, which led to the establishment of extreme greenhouse conditions towards the end of the period. It is widely considered that the activity of large igneous provinces (LIPs) such as the Emeishan LIP (~260-257 Ma) and the Siberian Traps (~252-250 Ma) would have played a major role in these changes, causing transient but dramatic increases in CO, that drove global warming levels and ocean acidity and anoxia to

TABLE 2. STRATIGRAPHIC AND PALEOENVIRONMENTAL EVOLUTION IN DIFFERENT SECTORS OF SW GONDWANA DURING THE LATE GUADALUPIAN-LOPINGIAN.

West	Stratigraphy and paleoenvironment	East
Intra-arc basins: El Tapado (this work)	Retroarc basins: Paganzo, Ischigualasto-Villa Unión (Gulbranson <i>et al.</i> , 2015; Spalletti and Limarino, 2017).	Intraplate basins: Paraná (Milani <i>et al.</i> , 2007; Holz <i>et al.</i> , 2010; Kern <i>et al.</i> , 2021).
El Tapado Formation: In the El Tapado section, carbonate and deepto-shallow volcaniclastic lacustrine deposits, followed by saline lacustrine and floodplain deposits, indicating an evolution from relatively humid to semi-arid or arid conditions. In the Las Tetas section, the transition from fluvial deposits to alluvial redbeds also points to increasing aridity.	Talampaya Formation: Clastic sequence comprising alluvial to fluvial deposits, followed by ephemeral fluvial, aeolian, and playa-lake deposits. A transition towards semi-arid to arid conditions is interpreted.	Pirambóia and Sanga do Cabral formations: Aeolian and fluvial redbedassociated with a desert climate. Rio do Rasto Formation: Lacustrine and deltaic plain deposits, transitioning to aeolian deposits developed under an arid climate.

Semi-arid to arid Climatic Stage according to the definition of Limarino et al. (2014).

peak, inducing the Guadalupian faunal crisis and the Permian-Triassic mass extinction (e.g., Joachimski et al., 2012; Limarino et al., 2014; Shellnut, 2014; Castillo et al., 2016). In this matter, it has been proposed that the sustained activity of the Choiyoi Magmatic Province could have also contributed to the generation of greenhouse conditions on a global scale through the input of large amounts of CO₂ (Limarino et al., 2014; del Rey et al., 2019), probably enhanced by the heating of organic-rich rocks (Spalletti and Limarino, 2017).

5.2. Guanaco Sonso Formation

In the Ingaguás section, the Guanaco Sonso Formation comprises lava flows, pyroclastic breccias, and lithic- and fine-rich tuffs, in an intermediate to acid compositional range, and is considered to represent the evolution of a volcanic terrain in a near-vent environment. The section displays vertical contrasts that suggest more than one emission source (e.g., associations VI3 and VM1; Fig. 3), setting a varied and fluctuating character in terms of the eruptive style and composition of the juvenile material, possibly as part of an intermediate to silicic multifocal complex (sensu Cas and Wright, 1987). In this latter case, diverse volcano types are possible, such as calderas and stratovolcanoes, located in large volcano-tectonic depressions commonly linked to

regional extensional faults (*e.g.*, Wolfe and Self, 1983; Aramaki, 1984; Busby and Bassett, 2007). An example of such is the succession of associations VI2 and L1 in the lower part of the Ingaguás section, deemed representative of caldera volcanism since it groups pyroclastic breccias formed by high-energy pyroclastic density currents, lacustrine sedimentation in ponding zones, lahar deposits, and dacitic lavas possibly associated with a post-caldera stage (*e.g.*, Lipman, 2000). Caldera-type activity has also been interpreted for the Guanaco Sonso Formation at ~29° S, where the unit is dominated by massive, eutaxitic tuffs with occurrence of lacustrine deposits (López *et al.*, 2015; Salazar and Coloma, 2016).

There are differences both in exposure and lithofacies associations between the volcanic products of the El Tapado and Guanaco Sonso formations. This is relevant as these records are respectively representative of the Middle to Late Permian and the Early to Middle Triassic volcanism in the region. The El Tapado Formation likely represents the inner to marginal zone of the Permian arc (Figs. 3 and 11), extending significantly to the east into Argentine territory with the Choiyoi Group. In turn, the Guanaco Sonso Formation shows a more internal (*i.e.*, nearvent) position within the Triassic arc. Given that the Guanaco Sonso rocks are abundant several tens of km west when compared to the El Tapado records, it is likely that during the Early Triassic the magmatic

arc migrated towards the edge of the continent at this latitude. This spatial relation also holds true when the intrusive Permian and Triassic rock records at around 30-30.5° S are analyzed (Velásquez *et al.*, 2021), possibly extending several hundred of kms north (*e.g.*, Maksaev *et al.*, 2014; Rocher *et al.*, 2015).

5.3. Regional stratigraphic relations

Hereunder, stratigraphic relations are presented between the sections analyzed in this work and those from other studies (Fig. 12). First, a local correlation is established between the El Tapado and Río Seco sections, as these two are within the study area. Then, regional relations are presented for the El Tapado and Guanaco Sonso formations.

Within the study area, at the headwaters of the Seco River (Fig. 2) outcrops a lacustrine succession described by Murillo et al. (2017), who preliminarily assigned it to the Jurassic Estratos de quebrada El Tapado Unit of Mpodozis and Cornejo (1988) based on one detrital zircon U-Pb age. Recently, Velásquez et al. (2021) recalculated this age, establishing it in 257.6±5.6 Ma (n=5), which is consistent with a U-Pb zircon age of 260±1.7 Ma obtained from an ignimbrite interbedded in the lacustrine succession of the El Tapado area (Figs. 3 and 12B). The stratigraphic evolution of the Río Seco and El Tapado areas is shown in figure 12B, where after an initial stage of low-energy carbonate sedimentation it follows a siliciclastic filling partially reworked by turbidity currents and flash floods, and a final stage dominated by fine sediments and evaporites. The paleoenvironment was likely a rather marginal intra-arc zone, particularly during the latest Guadalupian (Fig. 11).

At a regional scale, as presented in Section 5.1, the tectonic and depositional environment inferred for the El Tapado Formation presents important similarities with the Upper Section of the Choiyoi Group (Velásquez et al., 2021). The Upper Choiyoi is largely exposed in the Frontal Cordillera of Argentina and is characterized by voluminous ignimbrite volcanism, mostly rhyolitic in composition (Sato and Llambías, 1993; Llambías, 1999). At around 29.5 °S, Charchaflié (2003) reported U-Pb zircon ages of 263.7±0.7 Ma and 262.6±0.7 Ma in dacitic to rhyolitic tuffs assigned to the Choiyoi Group, which fall within the age range of the El Tapado Formation. Therefore, we support that this formation is representative of the Upper Section of the Choiyoi

Group in Chilean territory, as previously suggested by Velásquez *et al.* (2021). A proper correlation between these units is, however, still not possible due to the different lithostratigraphic criteria used, so a better understanding of the western reaches of the Choiyoi Magmatic Province following similar field methodologies will be an interesting next step.

A regional comparison can be established between the Las Tetas section and a section described by Rocher and Vallecillo (2014) in the Las Caletas area, Frontal Cordillera of San Juan, Argentina (~31.9° S), which is presented in figure 12A. The Las Caletas section comprises the Horcajo Formation, the youngest unit of the Choiyoi Group in that area and representative of its Upper Section. A U-Pb zircon age of 265±2 Ma was obtained in the upper part of this \sim 1,400 m-thick section by Rocher et al. (2015). This unit was likely deposited in an extensional setting, with tectonic (and volcano-tectonic) subsidence controlled by normal faults (Rocher and Abarzúa, 2013; Rocher and Vallecillo, 2014). Figure 12A shows that both areas are characterized by rhyolitic to dacitic volcanic deposits indicative of profuse caldera activity (e.g., welded ignimbrites, pyroclastic breccias, rhyolitic lava flows), along with sedimentation-dominated episodes associated with the reworking of these deposits. The stratigraphy of these two areas provides a consistent approach to the intra-arc environment during the Middle to Late Permian.

Looking into Chilean territory, it is worth noticing that the span of extensional activity interpreted in the study area (at least between ~263-257 Ma; Fig. 11) is almost coeval with the onset of the San Félix forearc rift basin at ~29° S, estimated at around 255 Ma, and which extended into the Middle Triassic (Salazar et al., 2020; see Section 2). Although further research is needed to understand the connection between these events, we think they represent an almost continuous timespan of extensional activity at a regional scale, consistent with the tectonic context of the pre-Andean Stage.

As for the Guanaco Sonso Formation, the main reference section was described at ~29° S by Salazar and Coloma (2016), who presented a U-Pb zircon age of 249.1±1.3 Ma. Figure 12C presents a comparison between this section and the Ingaguás section based on lithofacies associations. Both profiles are characterized by intercalations of dacitic welded ignimbrites and basaltic-andesitic lava packages, displaying an episodic character in terms of eruptive

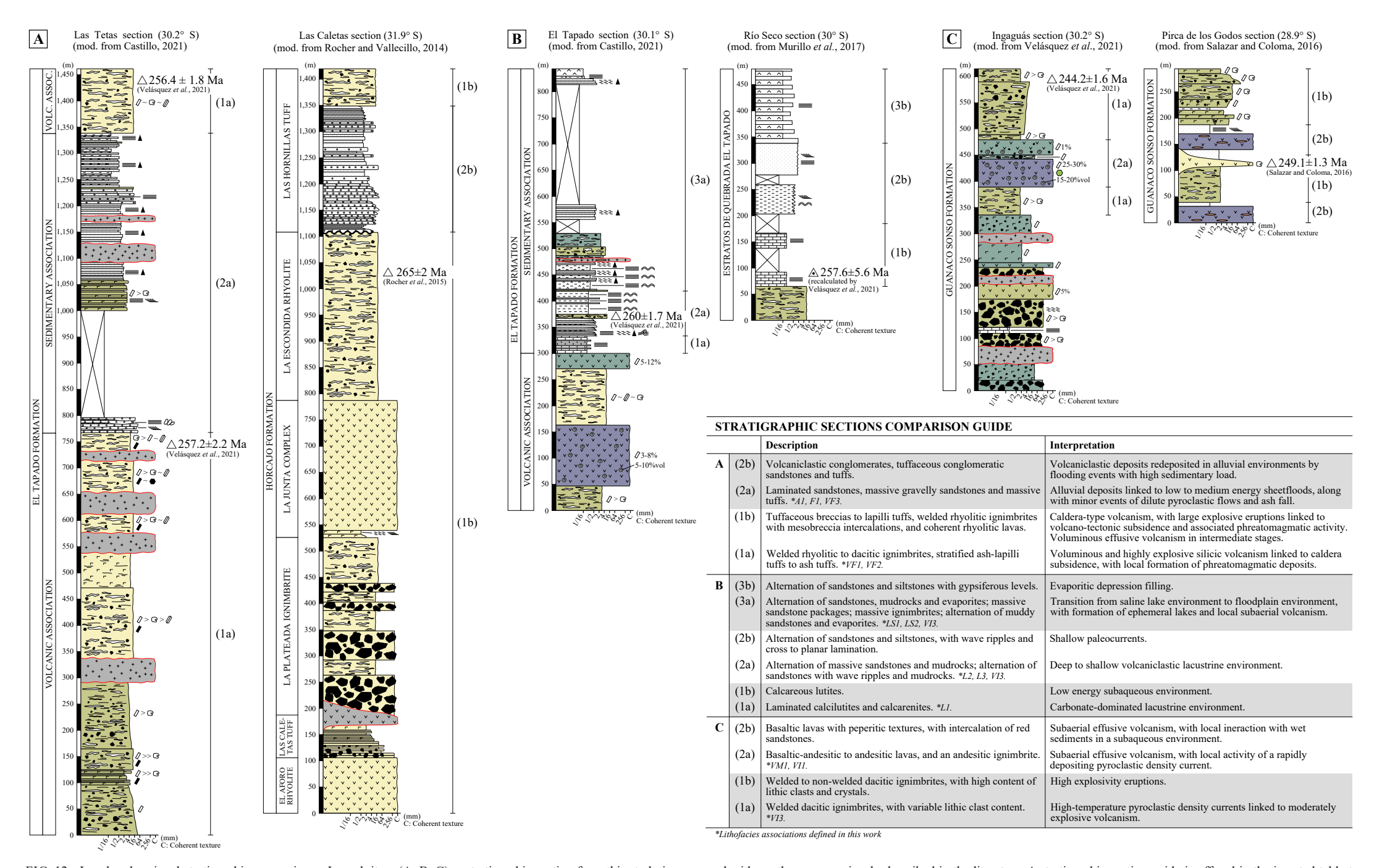


FIG. 12. Local and regional stratigraphic comparisons. In each item (A, B, C), a stratigraphic section from this study is compared with another one previously described in the literature. A stratigraphic section guide is offered in the inserted table to facilitate comparisons. A. Regional comparison between the El Tapado Formation in the Las Tetas area and the Horcajo Formation (Upper Section of the Choiyoi Group) in San Juan, Argentina, described by Rocher and Vallecillo (2014).

B. Local correlation between the El Tapado section and a succession of the Estratos de quebrada El Tapado Unit described by Murillo et al. (2017) in the Río Seco area (northern limit of our study area). C. Regional comparison between the Ingaguás section and the main reference section of the Guanaco Sonso Formation, described by Salazar and Coloma (2016) in the Pirca de los Godos area.

style and composition. In addition, López *et al.* (2015) and Salazar and Coloma (2016) interpreted caldera activity and local lacustrine sedimentation at ~29° S, which is also present in the study area. This comparison shows the consistency of the formation environment of the Guanaco Sonso Formation along its distribution in the Chilean Frontal Cordillera.

5.4. Permian-Triassic volcanism along SW Gondwana

The thick ignimbrites of the El Tapado Formation are related to high-explosivity, caldera-type volcanism typical of silicic volcanic complexes. From base to top, these deposits show progressively more silicic compositions, with an increasing presence of K-feldspar and hydrous minerals like amphibole and biotite (Fig. 3). This indicates a volatileenriching trend in the forming magmas that suggests advanced differentiation processes in the magmatic source. For the Upper Choiyoi ignimbrite record, advanced differentiation controlled by fractional crystallization has been inferred, associated with magmas emplaced in a relatively thin crust in the context of an extensional magmatic arc (Rocher et al., 2015). In turn, the Guanaco Sonso Formation also presents evidence of caldera-type volcanism, but with a less silicic composition. Dacitic ignimbrites are its most representative products, which up section give way to andesitic ignimbrites and then to dacitic ignimbrites again. The ignimbrites also intercalate with dacitic to basaltic-andesitic lavas. All these products represent volcanic episodes of varied and fluctuating composition and eruptive style, probably linked to intermediate to silicic volcanic complexes, indicative of a more dynamic and mature magmatic arc. This evolution trend is consistent with the following magmatic stage developed during the Late Triassic, represented in the Chilean Frontal Cordillera by basaltic-andesitic lavas and subordinate dacitic ignimbrites of the La Totora and San Félix formations (Salazar et al., 2013; Salazar and Coloma, 2016), and by bimodal successions of rhyolitic to dacitic ignimbrites and basaltic-andesitic lavas of the Pastos Blancos Formation (Ortiz and Merino, 2015; Murillo et al., 2017). Hence, the magmatism associated with the Guanaco Sonso Formation presents a transitional character between that typical of the Choiyoi Group and that characteristic of the last period of the pre-Andean Stage.

6. Conclusions

A stratigraphic description and lithofacies analysis, together with structural observations, have been carried out on volcanic and sedimentary rocks of the El Tapado and Guanaco Sonso formations, exposed in the La Laguna sector (~30-30.5° S), in the Chilean Frontal Cordillera. The obtained results provide relevant insights into the depositional, paleoenvironmental, and tectonic evolution of an intra-arc Permian-Triassic setting, as well as their regional significance when compared to the Choiyoi Magmatic Province.

The El Tapado Formation is characterized by rhyolitic to dacitic, thick and welded ignimbrites associated with caldera volcanism, present as the main filling of extensional depocenters within a volcanic landscape dominated by silicic volcanic centers. In the study area, the accommodation of this unit was likely related to extensional activity along major structures like the Olivares and Carmen faults. The occurrence of sedimentary episodes in this formation was primarily controlled by volcaniclastic input, as inferred in similar volcaniclastic basins elsewhere. The fluvial-alluvial post-eruptive successions observed in the eastern part of the study area were contemporary to a significant decrease in pyroclastic activity. In contrast, the lacustrine to subaerial sedimentation observed around the center of the study area was probably caused by a higher and more marginal position of this depocenter concerning the active emission centers. Sedimentary lithofacies associations suggest a transition from relatively humid conditions to semi-arid or even arid conditions during the Guadalupian-Lopingian, which is consistent with regional paleoclimatic observations and is the first evidence ever provided in a Gondwanan paleobasin in Chile. Based on the lithofacies analysis, the structural context, and available geochronological data, we consider that El Tapado Formation as representative of the Upper Section of the Choiyoi Group in Chilean territory, confirming previous assumptions.

The Guanaco Sonso Formation, which comprises andesitic to dacitic ignimbrites, breccias, and lavas, together with subordinate lacustrine and laharic deposits, constitutes a proximal (*i.e.*, near-vent) volcanic environment. In this formation, the varied and fluctuating nature of the volcanic products in terms of eruptive style and composition are interpreted

to represent an intermediate to silicic multifocal complex. These characteristics and interpretations are consistent with those reported at \sim 29° S, where its main reference section is located. The magmatic stage associated with the Guanaco Sonso Formation indicates a migration of the arc towards the continental margin (*i.e.*, trenchwards) at this latitude.

The volcanic products of the El Tapado and Guanaco Sonso formations differ notoriously in composition and eruptive style, setting a transition into the basaltic-andesitic to bimodal volcanism that would be characteristic of the last period of the pre-Andean Stage during the Late Triassic.

Acknowledgments

To the Plan Nacional de Geología of Sernageomin, for providing the support and resources for the development of this research as part a nationwide mapping program. To the geologist R. Velásquez, for his great willingness and accurate observations. To the geologists D. Villela and D. Mardónez, for their very important contributions in the field. And to F. Tapia and M.B. Yoya, whose revisions meant a significant improvement in the approach and quality of this study. This work is dedicated to the memory of Laura Varas, petrographer geologist, whose guidance was very valuable for the completion of this project, and whose professional and human excellence will continue to inspire us.

References

- Aramaki, S. 1984. Formation of the Aira caldera, southern Kyushu, ~22,000 years ago. Journal of Geophysical Research: Solid Earth 89 (B10): 8485-8501. https://doi.org/10.1029/JB089iB10p08485
- Ashmore, P. 1982. Laboratory modelling of gravel braided stream morphology. Earth Surface Processes and Landforms 7 (3): 201-225. https://doi.org/10.1002/ esp.3290070301
- Barredo, S.; Chemale, F.; Marsicano, C.; Ávila, J.; Ottone, E.; Ramos, V. 2012. Tectono-sequence stratigraphy and U-Pb zircon ages of the Rincón Blanco Depocenter, northern Cuyo Rift, Argentina. Gondwana Research 21 (2-3): 624-636. https://doi.org/10.1016/j.gr.2011.05.016
- Bastías-Mercado, F.; González, J.; Oliveros, V. 2020. Volumetric and compositional estimation of the Choiyoi Magmatic Province and its comparison with other Silicic Large Igneous Provinces. Journal of South American Earth Sciences 103: 102749. https://doi.org/10.1016/j.jsames.2020.102749
- Benvenuti, M. 2003. Facies analysis and tectonic significance of lacustrine fan-deltaic successions in the Pliocene-

- Pleistocene Mugello Basin, Central Italy. Sedimentary Geology 157 (3-4): 197-234. https://doi.org/10.1016/ S0037-0738(02)00234-8
- Blair, T.; McPherson, J. 1994. Alluvial fans and their natural distinction from rivers based on morphology, hydraulic processes, sedimentary processes, and facies assemblages. Journal of Sedimentary Research 64 (3a): 450-489. https://doi.org/10.1306/D4267DDE-2B26-11D7-8648000102C1865D
- Branney, M. 1991. Eruption and depositional facies of the Whorneyside Tuff Formation, English Lake District: An exceptionally large-magnitude phreatoplinian eruption. Geological Society of America Bulletin 103 (7): 886-897. https://doi.org/10.1130/0016-7606(1991)103%3C0 886:EADFOT%3E2.3.CO;2
- Branney, M.; Kokelaar, P. 2002. Pyroclastic density currents and the sedimentation of ignimbrites. Geological Society of London, Memoir 27: 143 p. London. https://doi.org/10.1144/GSL.MEM.2003.027
- Branney, M.; Kokelaar, B.; McConnell, B. 1992. The Bad Step Tuff: a lava-like rheomorphic ignimbrite in a calc-alkaline piecemeal caldera, English Lake District. Bulletin of Volcanology 54: 187-199. https://doi.org/10.1007/BF00278388
- Bryan, S.; Ewart, A.; Stephens, C.; Parianos, J.; Downes, P. 2000. The Whitsunday Volcanic Province, Central Queensland, Australia: lithological and stratigraphic investigations of a silicic-dominated large igneous province. Journal of Volcanology and Geothermal Research 99 (1-4): 55-78. https://doi.org/10.1016/S0377-0273(00)00157-8
- Bursik, M.; Woods, A. 1996. The dynamics and thermodynamics of large ash flows. Bulletin of Volcanology 58: 175-193. https://doi.org/10.1007/s004450050134
- Busby, C.; Bassett, K. 2007. Volcanic facies architecture of an intra-arc strike-slip basin, Santa Rita Mountains, Southern Arizona. Bulletin of Volcanology 70: 85-103. https://doi.org/10.1007/s00445-007-0122-9
- Cardó, R.; Díaz, I.; Cegarra, M.; Heredia, N.; Rodríguez Fernández, R.; Santamaría, G. 2005. Hoja Geológica 3169-I, Rodeo, Provincia de San Juan. Instituto de Geología y Recursos Minerales, Servicio Geológico Minero Argentino, Boletín 272: 47 p., 1 mapa escala 1:250.000. Buenos Aires.
- Cardó, R.; Díaz, I.; Limarino, O.; Litvak, V.; Poma, S.; Santamaría, G. 2007. Hoja Geológica 2969-III, Malimán, Provincias de San Juan y La Rioja. Instituto de Geología y Recursos Minerales, Servicio Geológico Minero Argentino, Boletín 320: 52 p., 1 mapa escala 1:250.000. Buenos Aires.

- Carroll, A.; Bohacs, K. 1999. Stratigraphic classification of ancient lakes: Balancing tectonic and climatic controls. Geology 27 (2): 99-102. https://doi.org/10.1130/0091-7613(1999)027%3C0099:SCOALB%3E2.3.CO;2
- Cas, R.; Wright, J. 1987. Volcanic Successions, Modern and Ancient: A geological approach to processes, products and successions. Allen and Unwin: 528 p. London.
- Cas, R.; Wright, J. 1991. Subaqueous pyroclastic flows and ignimbrites: an assessment. Bulletin of Volcanology 53: 357-380. https://doi.org/10.1007/BF00280227
- Castillo, D. 2021. Petrografía y análisis de facies de rocas estratificadas del Guadalupiano-Triásico Medio en la Cordillera Frontal de Elqui (29°58'-30°24'S), Región de Coquimbo, Chile. Memoria de título (Inédito). Universidad de Concepción, Departamento Ciencias de la Tierra: 155 p. Concepción.
- Castillo, P.; Fanning, C.; Hervé, F.; Lacassie, J. 2016. Characterisation and tracing of Permian magmatism in the south-western segment of the Gondwanan margin; U-Pb age, Lu-Hf and O isotopic compositions of detrital zircons from metasedimentary complexes of northern Antarctic Peninsula and western Patagonia. Gondwana Research 36: 1-13. https://doi.org/10.1016/j. gr.2015.07.014
- Charchaflié, D. 2003. Geological, structural and geochronological framework of the Veladero North area, Cordillera Frontal, Argentina. M.Sc. thesis (Unpublished), University of British Columbia: 125 p.
- Charrier, R.; Pinto, L.; Rodríguez, M. 2007. Tectonostratigraphic evolution of the Andean Orogen in Chile. *In* The Geology of Chile (Moreno, T.; Gibbons, W.; editors). Geological Society of London, Chapter 2: 21-114. London. https://doi.org/10.1144/GOCH.3
- Collinson, J. 1996. Alluvial sediments. *In* Sedimentary environments: processes, facies, and stratigraphy (3rd edition) (Reading, H.; editor). Blackwell Science: 37-82. Oxford.
- Coloma, F.; Valin, X.; Oliveros, V.; Vásquez, P.; Creixell, C.; Salazar, E.; Ducea, M. 2017. Geochemistry of Permian to Triassic igneous rocks from northern Chile (28°-30°15'S): Implications on the dynamics of the proto-Andean margin. Andean Geology 44 (2): 147-178. http://dx.doi.org/10.5027/andgeoV44n2-a03
- Cravero, O.; Herrmann, C.; Fauque, L.A.; Turel, A.V.; Johanis, P.E.; Moser, L.C. 2009. Carta Minero-Metalogenética 2969-I, Pastillos, Provincias de La Rioja y San Juan. Instituto de Geología y Recursos Minerales, Servicio Geológico Minero Argentino, Boletín 384: 91 p. Buenos Aires.
- D'Elia, L.; Muravchik, M.; Franzese, J.; López, L. 2012. Tectonostratigraphic analysis of the Late Triassic-

- Early Jurassic syn-rift sequence of the Neuquén Basin in the Sañicó depocentre, Neuquén Province, Argentina. Andean Geology 39 (1): 133-157. http://dx.doi.org/10.5027/andgeoV39N1-a07
- D'Elia, L.; Martí, J.; Muravchik, M.; Bilmes, A.; Franzese, J. 2016. Impact of volcanism on the sedimentary record of the Neuquén rift basin, Argentina: towards a cause and effect model. Basin Research 30 (S1): 311-335. https://doi.org/10.1111/bre.12222
- del Rey, A.; Deckart, K.; Arriagada, C.; Martínez, F. 2016. Resolving the paradigm of the late Paleozoic-Triassic Chilean magmatism: Isotopic approach. Gondwana Research 37: 172-181. https://doi.org/10.1016/j. gr.2016.06.008
- del Rey, A.; Deckart, K.; Planavsky, N.; Arriagada, C.; Martínez, F. 2019. Tectonic evolution of the southwestern margin of Pangea and its global implications: evidence from the mid Permian-Triassic magmatism along the Chilean-Argentine border. Gondwana Research 76: 303-321. https:// doi.org/10.1016/j.gr.2019.05.007
- Elliott, C.; Williams, P. 1988. Sediment slump structures: a review of diagnostic criteria and application to an example from Newfoundland. Journal of Structural Geology 10 (2): 171-182. https://doi.org/10.1016/0191-8141(88)90114-9
- Espinoza, M.; Montecino, D.; Oliveros, V.; Astudillo, N.; Vásquez, P.; Reyes, R.; Celis, C.; González, R.; Contreras, J.; Creixell, C.; Martínez, A. 2019. The synrift phase of the early Domeyko Basin (Triassic, northern Chile): Sedimentary, volcanic, and tectonic interplay in the evolution of an ancient subduction-related rift basin. Basin Research 31 (1): 4-32. https://doi.org/10.1111/bre.12305
- Dunham, R. 1962. Classification of carbonate rocks according to depositional texture. *In* Classification of Carbonate Rocks A Symposium (Ham, W.; editor). American Association of Petroleum Geologists, Memoir 1: 108-121. Tulsa.
- Eugster, H.; Hardie, L. 1978. Saline lakes. *In* Lakes: chemistry, geology, physics (Lerman, A.; editor). Springer-Verlag: 237-294. Berlin.
- Fauqué, L. 2010. Hoja Geológica 2969-I, Pastillos, Provincias de San Juan y La Rioja. Instituto de Geología y Recursos Minerales, Servicio Geológico Minero Argentino, Boletín 557.
- Folk, R. 1954. The distinction between grain size and mineral composition in sedimentary-rock nomenclature. The Journal of Geology 62 (4): 344-359.
- Folk, R. 1980. Petrology of sedimentary rocks. Hemphill Publishing Company: 182 p.

- Fosdick, J.; Carrapa, B.; Ortiz, G. 2015. Faulting and erosion in the Argentine Precordillera during changes in subduction regime: Reconciling bedrock cooling and detrital records. Earth and Planetary Science Letters 432: 73-83. https://doi.org/10.1016/j.epsl.2015.09.041
- Freundt, A. 1999. Formation of high-grade ignimbrites Part II. A pyroclastic suspension current model with implications also for low-grade ignimbrites. Bulletin of Volcanology 60: 545-567. https://doi.org/10.1007/s004450050251
- Gallego, O.; Breitkreuz, C. 1994. Conchostracos (Crustacea-Conchostraca) paleozoicos de la Región de Antofagasta, norte de Chile. Revista Geológica de Chile 21 (1): 31-53.
- Giambiagi, L.; Martínez, A. 2008. Permo-Triassic oblique extension in the Potrerillos-Uspallata area, western Argentina. Journal of South American Earth Sciences 26 (3): 252-260. https://doi.org/10.1016/j.jsames.2008.08.008
- Gianni, G.; Navarrete, C. 2022. Catastrophic slab loss in southwestern Pangea preserved in the mantle and igneous record. Nature Communications 13 (1): 698. https://doi.org/10.1038/s41467-022-28290-z
- González, J.; Oliveros, V.; Creixell, C.; Velásquez, R.; Vásquez, P.; Lucassen, F. 2018. The Triassic magmatism and its relation with the Pre-Andean tectonic evolution: Geochemical and petrographic constrains from the High Andes of north central Chile (29°30'-30°S). Journal of South American Earth Sciences 87: 95-112. https://doi.org/10.1016/j.jsames.2017.12.009
- Gulbranson, E.; Ciccioli, P.; Montañez, I.; Marenssi, S.; Limarino, C.; Schmitz, M.; Davydov, V. 2015. Paleoenvironments and age of the Talampaya Formation: The Permo-Triassic boundary in northwestern Argentina. Journal of South American Earth Sciences 63: 310-322. https://doi.org/10.1016/j.jsames.2015.08.008
- Hardie, L.; Smoot, J.; Eugster, H. 1978. Saline lakes and their deposits: a sedimentological approach. *In* Modern and ancient lake sediments, Vol. 2 (Matter, A; Tucker, M.E.; editors). International Association of Sedimentologists, Special Publication: 7-41. https://doi.org/10.1002/9781444303698.ch2
- Hein, F.; Walker, R. 1977. Bar evolution and development of stratification in the gravelly, braided, Kicking Horse River, British Columbia. Canadian Journal of Earth Sciences 14 (4): 562-570. https://doi.org/10.1139/ e77-058
- Heredia, N.; Fernández, L.; Gallastegui, G.; Busquets, P.; Colombo, F. 2002. Geological setting of the Argentine Frontal Cordillera in the flat-slab segment (30°00'-31°30'S latitude). Journal of South American Earth

- Sciences 15 (1): 79-99. https://doi.org/10.1016/ S0895-9811(02)00007-X
- Hernando, I.; Petrinovic, I.; Gutiérrez, D.; Bucher, J.; Fuentes, T.; Aragón, E. 2019. The caldera-forming eruption of the quaternary Payún Matrú volcano, Andean back-arc of the southern volcanic zone. Journal of Volcanology and Geothermal Research 384: 15-30. https://doi.org/10.1016/j.jvolgeores.2019.07.003
- Hervé, F.; Fanning, C.; Calderón, M.; Mpodozis, C. 2014.
 Early Permian to Late Triassic batholiths of the Chilean
 Frontal Cordillera (28-31°S): SHRIMP U-Pb zircon
 ages and Lu-Hf and O isotope systematics. Lithos 184:
 436-446. https://doi.org/10.1016/j.lithos.2013.10.018
- Holz, M.; França, A.; Souza, P.; Iannuzzi, R.; Rohn, R. 2010. A stratigraphic chart of the Late Carboniferous/ Permian succession of the eastern border of the Paraná Basin, Brazil, South America. Journal of South American Earth Sciences 29 (2): 381-399. https://doi.org/10.1016/j.jsames.2009.04.004
- Huang, Q.; Kamenetsky, V.; Ehrig, K.; McPhie, J.;
 Kamenetsky, M.; Cross, K.; Meffre, S.; Agangi, A.;
 Chambefort, I.; Direen, N.; Maas, R.; Apukhtina, O.
 2016. Olivine-phyric basalt in the Mesoproterozoic
 Gawler silicic large igneous province, South Australia:
 Examples at the Olympic Dam Iron Oxide Cu-U-Au-Ag deposit and other localities. Precambrian
 Research 281: 185-199. https://doi.org/10.1016/j.
 precamres.2016.05.019
- Joachimski, M.; Lai, X.; Shen, S.; Jiang, H.; Luo, G.; Chen, B.; Chen, J.; Sun, Y. 2012. Climate warming in the latest Permian and the Permian-Triassic mass extinction. Geology 40 (3): 195-198. https://doi. org/10.1130/G32707.1
- Jones, R.; Kirstein, L.; Kasemann, S.; Litvak, V.; Poma, S.; Alonso, R.; Hinton, R. 2016. The role of changing geodynamics in the progressive contamination of Late Cretaceous to Late Miocene arc magmas in the southern Central Andes. Lithos 262: 169-191. https:// doi.org/10.1016/j.lithos.2016.07.002
- Kern, H.; Lavina, E.; Paim, P.; Girelli, T.; Lana, C. 2021. Paleogeographic evolution of the southern Paraná Basin during the Late Permian and its relation to the Gondwanides. Sedimentary Geology 415: 105808. https://doi.org/10.1016/j.sedgeo.2020.105808
- Le Maitre, R.; Streckeisen, A.; Zanettin, B.; Le Bas, M.; Bonin, B.; Bateman, P. 2002. Igneous Rocks: A classification and glossary of terms: Recommendations of the International Union of Geological Sciences, Subcommission on the Systematics of Igneous Rocks (2nd edition). Cambridge University Press: 208 p. https://doi.org/10.1017/CBO9780511535581

- Limarino, C.; Césari, S.; Spalletti, L.; Taboada, A.; Isbell, J.; Geuna, S.; Gulbranson, E. 2014. A paleoclimatic review of southern South America during the late Paleozoic: a record from icehouse to extreme greenhouse conditions. Gondwana Research 25 (4): 1396-1421. https://doi.org/10.1016/j.gr.2012.12.022
- Lipman, P. 2000. Central San Juan caldera cluster: regional volcanic framework. *In* Ancient Lake Creede: its volcano-tectonic setting, history of sedimentation, and relation of mineralization in the Creede Mining District (Bethke, P.; Hay, R.; editors). Geological Society of America, Special Paper 346: 9-69. https://doi.org/10.1130/0-8137-2346-9.9
- Llambías, E. 1999. El magmatismo gondwánico durante el Paleozoico Superior-Triásico. Anales del Instituto de Geología y Recursos Minerales 29 (14): 349-376.
- Llambías, E.; Sato, A. 1995. El batolito de Colangüil: transición entre orogénesis y anorogénesis. Revista de la Asociación Geológica Argentina 50 (1-4): 111-131.
- Llambías, E.; Sato, A. 2011. Ciclo Gondwánico: la provincia magmática Choiyoi en Neuquén. *In* Congreso Geológico Argentino, No. 18, Relatorio: 53-62. Neuquén.
- Llambías, E.; Kleiman, L.; Salvarredi, J. 1993. El magmatismo gondwánico. *In* Congreso Geológico Argentino, No. 12, y Congreso de Exploración de Hidrocarburos, No. 2, Relatorio: 53-64. Mendoza.
- López, N.; Salazar, E.; Franco, C. 2015. Análisis de facies volcanoclásticas y control estructural de una sección de los Estratos de Guanaco Sonso, a los 29°S, Cordillera Frontal, Región de Atacama. *In* Congreso Geológico Chileno, No. 14, Actas I: 882-885. La Serena.
- Lossada, A.; Giambiagi, L.; Hoke, G.; Fitzgerald, P.; Creixell, C.; Murillo, I.; Mardónez, D.; Velásquez, R.; Suriano, J. 2017. Thermochronologic evidence for late Eocene Andean mountain building at 30°S. Tectonics 36 (11): 2693-2713. https://doi.org/10.1002/2017TC004608
- Lowenstein, T.; Hardie, L. 1985. Criteria for the recognition of salt-pan evaporites. Sedimentology 32 (5): 627-644. https://doi.org/10.1111/j.1365-3091.1985.tb00478.x
- Mackaman-Lofland, C.; Horton, B.; Fuentes, F.; Constenius, K.; Stockli, D. 2019. Mesozoic to Cenozoic retroarc basin evolution during changes in tectonic regime, southern Central Andes (31-33°S): Insights from zircon U-Pb geochronology. Journal of South American Earth Sciences 89: 299-318. https://doi.org/10.1016/j.jsames.2018.10.004
- Maksaev, V.; Munizaga, F.; Tassinari, C. 2014. Timing of the magmatism of the paleo-Pacific border of Gondwana: U-Pb geochronology of Late Paleozoic to Early Mesozoic igneous rocks of the north Chilean

- Andes between 20° and 31°S. Andean Geology 41 (3): 447-506. http://dx.doi.org/10.5027/andgeoV41n3-a01
- Malizia, D.; Limarino, C.; Sosa-Gómez, J.; Kokot, R.; Nullo, F.; Gutiérrez, P. 1999. Hoja Geológica 3169-2, Paso del Agua Negra, Provincia de San Juan. Instituto de Geología y Recursos Minerales, Servicio Geológico Minero Argentino, Boletín 288: 192 p., 1 mapa escala 1:100.000. Buenos Aires.
- Mazzarini, F.; Fornaciai, A.; Bistacchi, A.; Pasquarè, F. 2008. Fissural volcanism, polygenetic volcanic fields, and crustal thickness in the Payen Volcanic Complex on the central Andes foreland (Mendoza, Argentina). Geochemistry, Geophysics, Geosystems 9: Q09002. https://doi.org/10.1029/2008GC002037
- McPhie, J. 1986. Primary and redeposited facies from a large-magnitude, rhyolitic, phreatomagmatic eruption: Cana Creek Tuff, Late Carboniferous, Australia. Journal of Volcanology and Geothermal Research 28 (3-4): 319-350. https://doi.org/10.1016/0377-0273(86)90029-6
- McPhie, J.; Doyle, M.; Allen, R. 1993. Volcanic textures: A guide to the interpretation of textures in volcanic rocks. Centre for Ore Deposit and Exploration Studies, University of Tasmania: 196 p. Hobart.
- Melchor, R.; Cardonatto, M.; Visconti, G. 2012.
 Palaeonvironmental and palaeoecological significance of flamingo-like footprints in shallow-lacustrine rocks: an example from the Oligocene-Miocene Vinchina Formation, Argentina. Palaeogeography, Palaeoclimatology, Palaeoecology 315-316: 181-198. https://doi.org/10.1016/j.palaeo.2011.12.005
- Miall, A. 2006. The geology of fluvial deposits: Sedimentary facies, basin analysis, and petroleum, geology. Springer-Verlag: 582 p. Berlin.
- Milani, E.; Melo, J.; Souza, P.; Fernandes, L.; França, A. 2007. Bacia do Paraná. Boletim de Geociencias-Petrobras 15 (2): 265-287.
- Moscoso, R.; Mpodozis, C. 1988. Estilos estructurales en el norte chico de Chile (28-31° S), regiones de Atacama y Coquimbo. Andean Geology 15 (2): 151-166.
- Mpodozis, C.; Cornejo, P. 1988. Hoja Pisco Elqui, Región de Coquimbo. Servicio Nacional de Geología y Minería, Carta Geológica de Chile, Serie Geología Básica 68: 164 p., 1 mapa escala 1:250.000. Santiago.
- Mpodozis, C.; Kay, S. 1992. Late Paleozoic to Triassic evolution of the Gondwana margin: Evidence from Chilean Frontal Cordilleran batholiths (28°S to 31°S). Geological Society of America Bulletin 104 (8): 999-1014. https://doi.org/10.1130/0016-7606(1992)104%3C0 999:LPTTEO%3E2.3.CO;2

- Murillo, I.; Velásquez, R.; Creixell, C. 2017. Geología de las áreas Guanta-Los Cuartitos y Paso de Vacas Heladas, regiones de Atacama y de Coquimbo. Servicio Nacional de Geología y Minería, Carta Geológica de Chile, Serie Geología Básica 192-193: 96 p., 1 mapa escala 1:100.000. Santiago.
- Nichols, G. 2009. Sedimentology and Stratigraphy (2nd edition). Wiley-Blackwell: 419 p. Hoboken.
- Oliveros, V.; Vásquez, P.; Creixell, C.; Lucassen, F.; Ducea, M.; Ciocca, I.; González, J.; Espinoza, M.; Salazar, E.; Coloma, F.; Kasemann, S. 2020. Lithospheric evolution of the Pre- and Early Andean convergent margin, Chile. Gondwana Research 80: 202-227. https://doi.org/10.1016/j.gr.2019.11.002
- Ortiz, M.; Merino, R. 2015. Geología de las áreas Río Chollay-Matancilla y Cajón del Encierro, regiones de Atacama y Coquimbo. Servicio Nacional de Geología y Minería, Carta Geológica de Chile, Serie Geología Básica 175-176: 234 p., 1 mapa escala 1:100.000. Santiago.
- Owen, L.; Windley, B.; Cunningham, W.; Badamgarav, J.; Dorjnamjaa, D. 1997. Quaternary alluvial fans in the Gobi of southern Mongolia: evidence for neotectonics and climate change. Journal of Quaternary Science 12 (3): 239-252. https://doi.org/10.1002/(SICI)1099-1417(199705/06)12:3%3C239::AID-JQS293%3E3.0.CO;2-P
- Pankhurst, R.; Leat, P.; Sruoga, P.; Rapela, C.; Márquez, M.; Storey, B.; Riley, T. 1998. The Chon Aike province of Patagonia and related rocks in West Antarctica: a silicic large igneous province. Journal of Volcanology and Geothermal Research 81 (1-2): 113-136. https:// doi.org/10.1016/S0377-0273(97)00070-X
- Rajchl, M.; Uličný, D.; Mach, K. 2008. Interplay between tectonics and compaction in a rift-margin, lacustrine delta system: Miocene of the Eger Graben, Czech Republic. Sedimentology 55 (5): 1419-1447. https://doi.org/10.1111/j.1365-3091.2008.00951.x
- Rocher, S.; Abarzúa, F. 2013. Interpretación litofacial en depósitos volcaniclásticos resedimentados asociados al volcanismo explosivo permo-triásico de la Cordillera Frontal de San Juan, oeste de Argentina. *In* Latin American Congress of Sedimentology, No 6, Proceedings: p. 85. São Paulo.
- Rocher, S.; Vallecillo, G. 2014. Mecanismos eruptivos y procesos depositacionales del Grupo Choiyoi en el área de Las Caletas, Cordillera Frontal de San Juan, Argentina. Andean Geology 41 (3): 589-625. http://dx.doi.org/10.5027/andgeoV41n3-a05
- Rocher, S.; Vallecillo, G.; Castro de Machuca, B.; Alasino, P. 2015. El Grupo Choiyoi (Pérmico temprano-medio) en

- la Cordillera Frontal de Calingasta, San Juan, Argentina: volcanismo de arco asociado a extensión. Revista Mexicana de Ciencias Geológicas 32 (3): 415-432.
- Salazar, E. 2012. Evolución tectonoestratigráfica de la cordillera de Vallenar: Implicancias en la construcción del oroclino de Vallenar. Tesis de Magíster (Inédito). Universidad de Chile, Departamento de Geología: 126 p., 1 mapa escala 1:100.000.
- Salazar, E.; Coloma, F. 2016. Geología del área Cerro de Cantaritos-Laguna Chica, Región de Atacama. Servicio Nacional de Geología y Minería, Carta Geológica de Chile, Serie Geología Básica 181: 171 p., 1 mapa escala 1:100.000. Santiago.
- Salazar, E.; Coloma, F.; Creixell, C. 2013. Geología del área El Tránsito-Lagunillas, Región de Atacama. Servicio Nacional de Geología y Minería, Carta Geológica de Chile, Serie Geología Básica 149: 117 p., 1 mapa escala 1:100.000. Santiago.
- Salazar, E.; Vásquez, P.; Vallejos, D.; Creixell, C.; Oliveros, V.; Ducea, M. 2020. Stratigraphic and provenance analysis of Triassic rock units between 28-29° S, northern Chile: implications on the tectonic and paleogeographic evolution of the southwestern margin of Gondwana. Andean Geology 47 (2): 207-255. http://dx.doi.org/10.5027/andgeoV47n2-3118
- Sato, A.; Llambías, E.J. 1993. El Grupo Choiyoi, provincia de San Juan: equivalente efusivo del Batolito de Colangüil. *In* Congreso Geológico Argentino, No. 12, y Congreso de Exploración de Hidrocarburos, No. 2, Actas 4: 156-165. Mendoza.
- Sato, A.; Llambías, E.; Basei, M.; Castro, C. 2015. Three stages in the Late Paleozoic to Triassic magmatism of southwestern Gondwana, and the relationships with the volcanogenic events in coeval basins. Journal of South American Earth Sciences 63: 48-69. https://doi.org/10.1016/j.jsames.2015.07.005
- Self, S. 1983. Large-scale phreatomagmatic silicic volcanism: A case study from New Zealand. Journal of Volcanology and Geothermal Research 17 (1-4): 433-469. https://doi.org/10.1016/0377-0273(83)90079-3
- Self, S.; Sparks, R. 1978. Characteristics of widespread pyroclastic deposits formed by the interaction of silicic magma and water. Bulletin of Volcanology 41: 196-212. https://doi.org/10.1007/BF02597223
- Shellnutt, J.G. 2014. The Emeishan large igneous province: A synthesis. Geoscience Frontiers 5 (3): 369-394. https://doi.org/10.1016/j.gsf.2013.07.003
- Smith, G.; Lowe, D. 1991. Lahars: volcano-hydrologic events and deposition in the debris flow - hyperconcentrated flow continuum. *In Sedimentation in Volcanic Settings* (Fisher, R.; Smith, G.; editors). SEPM Society for

- Sedimentary Geology, Special Publication 45: 59-70. Tulsa. https://doi.org/10.2110/pec.91.45.0059
- Smith, S. 1990. The sedimentology and accretionary styles of an ancient gravel-bed stream: the Budleigh Salterton Pebble Beds (Lower Triassic), southwest England. Sedimentary Geology 67(3-4): 199-219. https://doi.org/10.1016/0037-0738(90)90035-R
- Spalletti, L.; Limarino, C. 2017. The Choiyoi magmatism in south western Gondwana: implications for the end-permian mass extinction a review. Andean Geology 44 (3): 328-338. http://dx.doi.org/10.5027/andgeoV44n3-a05
- Sparks, R.; Tait, S.; Yanev, Y. 1999. Dense welding caused by volatile resorption. Journal of the Geological Society 156 (2): 217-225. https://doi.org/10.1144/ gsjgs.156.2.0217
- Sulpizio, R.; Dellino, P. 2008. Sedimentology, depositional mechanisms and pulsating behaviour of pyroclastic density currents. *In* Caldera Volcanism: Analysis, Modelling and Response (Gottsman, J.; Martí, J.; editors). Developments in Volcanology 10: 57-96. Amsterdam. https://doi.org/10.1016/S1871-644X(07)00002-2
- Talbot, J.; Self, S.; Wilson, C. 1994. Dilute gravity current and rain-flushed ash deposits in the 1.8 ka Hatepe Plinian deposit, Taupo, New Zealand. Bulletin of Volcanology 56: 538-551. https://doi.org/10.1007/ BF00302834

- Talbot, M.; Allen, P. 1996. Lakes. *In* Sedimentary environments: processes, facies, and stratigraphy (3rd edition) (Reading, H.; editor). Blackwell Science: 83-124. Oxford.
- Thompson, A. 1986. Secondary flows and the poolriffle unit: A case study of the processes of meander development. Earth Surface Processes and Landforms 11 (6): 631-641. https://doi.org/10.1002/esp.3290110606
- Tucker, M. 2003. Sedimentary rocks in the field (3rd edition). John Wiley & Sons: 234 p. Chichester.
- Velásquez, R.; Coloma, F.; Murillo, I.; Merino, R.; Ortiz, M. 2021. Geología de las áreas Pisco Elqui y Paso del Agua Negra, región de Coquimbo. Servicio Nacional de Geología y Minería, Carta Geológica de Chile, Serie Geología Básica 211-212: 201 p., 1 mapa escala 1:100.000. Santiago.
- Walker, G. 1971. Grain-size characteristics of pyroclastic deposits. The Journal of Geology 79 (6): 696-714.
- Walker, G. 1981. Characteristics of two phreatoplinian ashes, and their water-flushed origin. Journal of Volcanology and Geothermal Research 9 (4): 395-407. https://doi.org/10.1016/0377-0273(81)90046-9
- Wolfe, J.; Self, S. 1983. Structural lineaments and Neogene volcanism in southwestern Luzon. *In* The tectonic and geologic evolution of southeast Asian seas and islands: Part 2 (Hayes, D.; editor). Geophysical Monograph Series 27: 157-172. https://doi.org/10.1029/GM027p0157

Manuscript received: August 11, 2023; revised/accepted: October 21, 2024; available online: November 05, 2024.

Appendix A: Stratigraphy and lithofacies analysis

1. Stratigraphic sections

A general description of the stratigraphic sections is presented.

1.1. Las Tetas section

This section is a composite of two nearby transects described west of the Colorado river, in the hanging wall of the Olivares fault, on rocks of the El Tapado Formation (Fig. 2). The lower transect corresponds to an \sim 800 m-thick homocline with a dip of \sim 30° to the northwest, comprising from the dacitic ignimbrites of VF1 to the fluvial conglomerates of F1 (Fig. 3), which are truncated by the Olivares fault. The upper transect is located a few hundred meters to the southwest of the lower transect. A \sim 200 m-thick stratigraphic gap is estimated between the two on the basis of field and remote (e.g., geospatial) observations. The upper transect consists of a homocline dipping subvertically to the northwest, comprising from the stratified pyroclastic deposits of VF3 to the rhyolitic ignimbrites of VF1 (Fig. 3), which are also truncated by the Olivares fault. Both transects are intruded by several aplitic sills.

Coordinates (SIRGAS UTM Zone 19S):

- Lower transect:
 - Bottom: N 6,661,950 m; E 413,570 m
 - Top: N 6,662,690 m; E 412,670 m
- Upper transect:
 - Bottom: N 6,660,890 m; E 411,360 m
 - Top: N 6,661,060 m; E 410,810 m

1.2. El Tapado section

This section was described to the north of the El Tapado ravine, in the footwall of the Carmen fault (Fig. 2). It consists of a succession of ignimbrites, lavas, and thick lacustrine to subaerial deposits of the El Tapado Formation. The rocks form a homocline that dips gently to the southeast and is interrupted by the Carmen fault, which brings it into contact with an almost coeval pyroclastic succession of the El Tapado Formation (Fig. 4A).

Coordinates (SIRGAS UTM Zone 19S):

- Bottom: N 6,672,280 m; E 403,340 m
- Top: N 6,671,640 m; E 404,530 m

1.3. Ingaguás section

This section, modified from Velásquez *et al.* (2021), was described on the east side of the Ingaguás river valley, east of the Matusalén ravine, in the footwall of the Baños del Toro fault (Fig. 2). It comprises lavas, pyroclastic deposits, and sparse sedimentary rocks of the Guanaco Sonso Formation, forming a gently dipping homocline to the west. The succession is intruded by monzogranitic sills and is in contact towards the top with the Piuquenes Plutonic Complex.

Coordinates (SIRGAS UTM Zone 19S):

- Bottom: N 6,658,110 m; E 391,040 m
- Top: N 6,658,270 m; E 392,520 m

2. Lithofacies associations

Below is a detailed description and interpretation for each lithofacies association defined in this work. Mention is made to lithofacies codes, figures, tables, and references presented in the main body of this article.

2.1. Volcanic lithofacies associations

2.1.1. Mafic volcanism

VM1: Basaltic-andesitic to andesitic lavas (cB, cA)

Description: Packages of meter-scale coherent basaltic-andesitic (lithofacies *cB*) to andesitic (lithofacies *cA*) lavas. In the El Tapado section, they are dark gray to black in color and have mostly porphyritic texture, with 3-12% phenocrysts of 1-2 mm of plagioclase and subordinate amphibole in an aphanitic groundmass. Other subordinate layers are aphanitic in texture. The packages show decimeter-scale columnar jointing, and flow textures given by tight and sinuous fractures subparallel to the stratification plane. The lower package has an amygdaloidal texture, with zeolites and calcite filling (Fig. 4B). Thicknesses are maximum in the section and decrease laterally until their trace is lost a several tens of meters away.

In the Ingaguás section, the cB lavas are dark gray to greenish gray in color and have porphyritic and amygdaloidal texture. Most of them have 25-30% plagioclase phenocrysts in an aphanitic groundmass, and amygdules (\sim 15-20%vol.) of calcite, zeolite and clays. Other layers have olivine phenocrysts (4-13%) in a subophitic to intersertal groundmass of clinopyroxene, plagioclase and iron oxides, with sparse and small calcite amygdules. cA consists of slightly porphyritic lavas, with phenocrysts (\sim 1%) of plagioclase in an aphanitic groundmass. Locally, they include volcanic lithics and calcite amygdules towards their base.

Interpretation: This lithofacies association represents subaerial mafic to intermediate effusive volcanism (e.g., McPhie et al., 1993). The thickness variations observed in the El Tapado section suggest a high proximity to the emission center. In turn, columnar jointing is attributed to tensional stresses in the lava flows due to contraction during cooling (e.g., Cas and Wright, 1987). The composition, phenocryst content, and vesicular texture of the lavas indicate low viscosity magmas, with a relatively high degree of volatile exsolution in the case of cB (e.g., McPhie et al., 1993).

2.1.2. Intermediate volcanism

VI1: Proximal andesitic volcanism (mBr, mlLT, frmT, cA)

Description: This association groups massive pyroclastic breccias (lithofacies mBr), lithic-rich massive ash-lapilli tuffs (lithofacies mlLT), fine-rich massive ash tuffs (lithofacies frmT), and subordinate andesitic lavas (lithofacies cA). Three packages of this association are recognized in the Ingaguás section. The lower package groups massive pyroclastic breccias (mBr) and lithic-rich massive ash-lapilli tuffs (mlLT). The breccias of mBr are greenish to dark gray in color, matrix-supported, poorly to very poorly sorted, consist essentially of polymictic volcanic lithics in a glassy matrix and show alteration of propylitic affinity. The ignimbrites of mlLT are gray in color, matrix-supported, poorly to very poorly sorted, and contain lithics of light shades, corresponding to intrusives and tuffs, in a matrix of fine vitreous ash.

The middle package is composed of an andesitic lava (*cA*), a fine-rich massive ash tuff (*frmT*), and a lithic-rich massive ash-lapilli tuff (*mlLT*). *cA* is greenish to dark gray in color and has a porphyritic texture, with scarce plagioclase phenocrysts in an aphanitic groundmass. *frmT* is dark gray in color, matrix-supported, poorly sorted, and contains 30-35% plagioclase crystals in a matrix of fine vitreous ash, being classified as vitric in terms of fragment composition. Finally, *mlLT* is gray in color and contains abundant volcanic lithics 2-3 cm in diameter and plagioclase crystals, in a matrix of fine vitreous ash.

The upper package consists of a massive lithic-rich ash-lapilli tuff (*mlLT*). It has a reddish-brown color and contains 25-30% and esitic lithics up to 4 cm in diameter, with elongated to equidimensional shapes, diffuse to well-defined rounded edges, and variable crystallinity grade (*i.e.*, juvenile lithics; Fig. 4C). Other lithics (10-15%) are up to 1 cm in diameter, angular and of intermediate to felsic volcanic type (accidental or accessory). The glassy matrix has incipient to moderate welding and includes 25-35% plagioclase crystals.

Interpretation: This association is interpreted as proximal (*i.e.*, near-vent) volcanic deposits derived from mainly explosive andesitic volcanism, precursor of high-energy pyroclastic density currents. The massive structure and poor sorting of the pyroclastic deposits (*mBr*, *mlLT*, *frmT*) point to fluid escape as the dominant depositional control, which can be attributed to their abundant fine fraction (low permeability) or to a high gas content in the current (*e.g.*, Branney and Kokelaar, 2002; Sulpizio and Dellino, 2008). *frmT* is interpreted as a smaller grain-size equivalent of *mLT*, formed by pyroclastic density currents of lower concentration, depleted in lithics. The succession *cA-frmT-mlLT* in the middle part of the Ingaguás section denotes a progressive enrichment in volatiles of the magmatic source, probably associated with an injection of new magma, capable of inducing the transition from effusivity to increasing explosivity. For the *mlLT* layer in the upper part of the section, the variable shape, texture and crystallinity grade of its juvenile lithics suggest differences in magma rheology, which may be associated with magmatic chamber zonation (*e.g.*, Hernando *et al.*, 2019). Mineral content in all lithofacies suggests overall andesitic compositions.

VI2: Proximal dacitic volcanism (cD, mBr, mBrf, dbBrf, Sm, Ll)

Description: Massive pyroclastic breccias (mBr) and massive to diffusely bedded pyroclastic breccias with directional grain fabric (mBrf, dbBrf) of dacitic composition, intercalated with dacitic lavas (cD), massive sandstones (Sm), and redeposited calcilutites (Ll). mBr is reddish-gray, matrix-supported and poorly sorted, with decimeter to centimeter-scale clasts of mainly felsic intrusive rocks. mBrf and dbBrf have decimeter to meter-scale layers that are reddish-gray, matrix-supported (with some clast-supported domains), and poorly sorted, although better than mBr. Their directional fabric is defined by blocks and lapilli with their long axes parallel to the bedding plane, and they develop inverse lithic gradation (Fig. 4D). In terms of components, there are lithics (35-80%) of ~ 8 cm in diameter on average $(\sim 1$ m maximum) of intrusive, lavic and tuffaceous type to a lesser extent, in addition to juvenile lithics (5-15%), centimeter to decimeter-scale in diameter, and crystals (5-10%) of plagioclase and quartz in similar proportion, in a matrix of fine vitreous ash (5-40%). In the lower part of the Ingaguás section, the breccias are capped by levels of stratified calcilutites <25 cm thick (Fig. 4D), which have tabular to irregular shape, abrupt changes in thickness, and are partially mixed with the vitreous ash matrix. cD consists of meter-scale massive lava flows of red color, slightly porphyritic in texture, with small and scarce plagioclase phenocrysts. In turn, Sm is composed of fine- to medium-grained sandstones, arranged in centimeter- to decimeter-scale tabular layers of gray color.

Interpretation: The dacitic volcanites of this association are considered to represent an evolution from a stage of high-energy explosive volcanism (breccias) to one of lava effusion, probably linked to intense degassing of the magmatic source (e.g., Cas and Wright, 1987). The poor sorting and massive structure of mBr point to fluid escape as the dominant control in the lower part of the current during deposition (e.g., Branney and Kokelaar, 2002), whereas the breccias with directional grain fabric and diffuse bedding (mBrf+dbBrf) indicate a greater influence of the granular flow component, through shearing and energy transfer between clasts, a mechanism that also explains the inverse gradation of lithics through combined processes of kinetic sieving and kinematic squeezing (e.g., Branney and Kokelaar, 2002; Sulpizio and Dellino, 2008). These characteristics fit the pulsational model of Sulpizio and Dellino (2008) for low-volume pyroclastic density currents, in which deposition would occur through successive pulses stopped en masse. In particular, it is inferred that the irregular calcilutite levels in the breccias would have been removed in a semi-consolidated state by the current and transported to the top of each pulse by buoyancy effects. The sandstones (Sm) intercalated in the breccias are attributable to intermittent laharic events during pyroclastic activity, probably through hyperconcentrated flows, as suggested by their tabular geometry and massive structure (e.g., Smith and Lowe, 1991). Mineral content of the volcanic lithofacies suggests overall dacitic compositions.

VI3: Andesitic to dacitic ignimbrites (emLT, mLT, efrmT)

Description: Massive, mostly eutaxitic ash-lapilli to lapilli-ash tuffs (*emLT*, *mLT*) and massive, eutaxitic, fine-rich ash tuffs (*efrmT*), of andesitic to dacitic composition. All lithofacies are poorly to very poorly sorted.

In the El Tapado section, a succession of three eutaxitic lapilli-ash tuffs (*emLT*) is recognized. They are conformed mainly by vitric fragments, have andesitic to dacitic compositions, and violaceous to yellowish-gray colors. The first ignimbrite has incipient welding and contains 10-15% *fiamme* up to 5 mm long, 8-13% plagioclase and amphibole crystals, and 1-3% angular lava lithics up to 2 mm long, enveloped in a slightly vesicular glassy matrix. The second ignimbrite has moderate to penetrative welding and consists of 10-15%

fiamme up to 5 cm long, 15-20% plagioclase, quartz and amphibole crystals, and 7-12% angular lava lithics up to 3 cm in diameter (some with concave edges), in a glassy matrix with numerous lithophyses 1-3 mm in diameter. The third ignimbrite (Fig. 4E), in turn, has moderate welding and contains 12-23% fiamme up to 4 cm long, 18-23% plagioclase and amphibole crystals, and 1-2% angular lava lithics up to 2 mm in diameter, enveloped in a glassy matrix.

Lower in the El Tapado section, there are other two ignimbrites: one intercalated between deposits of lacustrine associations L2 and L3, and the other intercalated between L3 and LS1 (Fig. 3), both corresponding to massive vitric lapilli-ash tuffs (mLT). The former has incipient welding, irregular to flattened vitreous juvenile pyroclasts, plagioclase, quartz and sanidine crystals, and angular lava and tuffaceous lithics, in a matrix of vitreous fine ash and slightly flattened glass shards (Fig. 4F). The latter has rounded pumice, plagioclase and quartz crystals, and angular lava and tuffaceous lithics.

In the upper half of the Ingaguás section, eutaxitic, fine-rich, massive ash tuffs (*efrmT*) and eutaxitic, massive ash-lapilli tuffs (*emLT*) of dacitic juvenile composition are recognized. *efrmT* is brownish red in color, has 25-35% plagioclase and minor quartz crystals, along with *fiamme* (5-10%) up to 1 cm long, and sparse angular volcanic lithics up to 3 mm in diameter, in a matrix of fine vitreous ash and moderately welded glass shards (Fig. 4G). *emLT* is also brownish red in color and contains abundant lithics up to 15 mm in diameter, of lava and subordinate intrusive type, which present inverse gradation. There are also *fiamme* up to 4 mm long, and pervasively altered crystals, in a matrix of fine vitreous ash.

Interpretation: Explosive intermediate volcanic products, whose high proportion of fine vitreous ash, eutaxitic texture, and massive structure, denote an origin from high-temperature pyroclastic density currents, with deposition controlled by fluid escape (*e.g.*, Branney and Kokelaar, 2002). The smaller grain-size and lithic depletion of the ignimbrites of *efrmT* is attributed to a relatively lower concentration of the forming current. The inverse lithic gradation of *emLT* in the Ingaguás section may be linked to increased current competence, or lithic availability, for example, as a result of proximal avalanches (*e.g.*, Branney and Kokelaar, 2002).

In the El Tapado section, this intermediate volcanism is recorded from the redeposited pyroclastic deposits of underlying lacustrine associations L2 and L3. The ignimbrite intercalated between associations L2 and L3 is surrounded by deep and shallow lacustrine deposits, respectively, so it is very likely to have been emplaced in a subaqueous environment. Its incipient welding and flattened juvenile pyroclasts point to hot deposition, which restricts its emplacement to shallow waters (e.g., Cas and Wright, 1991). As for the upper package of emLT ignimbrites in the El Tapado section, their texture indicates subaerial deposition, which is consistent with the lacustrine to subaerial environment inferred for the underlying association LS1.

2.1.3. Felsic volcanism

VF1: Dacitic to rhyolitic ignimbrites (emLT, emlLT, //sT, mT)

Description: Decimeter- to meter-scale ash lapilli to lapilli-ash tuffs, massive in structure and eutaxitic in texture (emLT), with mostly moderate to dense welding (Fig. 5A to C). Some subordinate levels of these ash lapilli to lapilli-ash tuffs are enriched in lithic fragments (emlLT). Locally, thin (cm-thick) layers of parallel-stratified ash tuffs (//sT) and massive ash tuffs (mT) crown the ignimbrites.

This association is the most abundant in the Las Tetas section. There, their color varies mostly between light pink, orange, light gray, and whitish. They contain 15-30% (up to 40%) of *fiamme* up to ~15 cm long, generally very flattened by welding (Fig. 5B and C), and locally with amoeboid shapes (Fig. 5D). There are also polymictic volcanic lithic fragments up to 5 cm in diameter, whose proportion does not exceed 15%, except for subordinate layers where they reach 35-40%, characterizing these layers as lithic-enriched (*emlLT*). Lithics are of lava and tuffaceous type, and most of them are angular and with well-defined edges, so they are considered accidental or accessory. In some segments of the section (Fig. 3) they are normally graded in proportion and size. The crystalline fraction is 5-15% in several deposits, reaching 25-35% in other ignimbrites. Crystals are mainly plagioclase, quartz and sanidine; ferromagnesian crystals are subordinate, finding amphibole and biotite (Fig. 3). All of the above is supported by a matrix of abundant fine vitreous ash. Juvenile composition is estimated as dacitic to rhyolitic, showing a progressive increase in silica content towards the top of the section.

In the uppermost part of the Las Tetas section, eutaxitic, massive lapilli-ash tuffs (*emLT*) are recognized. They are conformed mainly by vitric fragments, have moderate welding, strong red color with brownish tone, and a composition estimated as rhyolitic. They contain 20-35% *fiamme* up to 6 cm long, with irregular, sinuous shapes, and argillaceous halos. There are also 15-25% of plagioclase, quartz and sanidine crystals, in similar proportions, in addition to 2-3% of lithic fragments up to 2 cm in diameter, angular and with well-defined edges, of lava and tuffaceous type. Under the microscope, it is observed that the matrix is composed mostly of glass shards, flattened and deformed around larger fragments (Fig. 5C).

In the lower part of the El Tapado section, eutaxitic, massive lapilli-ash tuffs (*emLT*) are observed. They are conformed mainly by vitric fragments, have moderate to dense welding, and light gray color with brownish to yellowish tone. They consist of abundant vitreous material, with 50-70% of vitreous fine ash matrix and flattened glass shards, and 25-30% of *fiamme* up to 12 cm long, flattened and deformed around other fragments. There are also 5-20% of plagioclase, quartz and sanidine crystals, in similar proportions. Subordinately, there are volcanic lithic fragments (1-3%) up to 2 cm in diameter, angular and with well-defined edges, frequently with concave, irregular or rough shapes, and argillaceous halos.

Interpretation: The poor sorting and massive structure of ignimbrites suggest that the dominant depositional control is the escape of fluids from the forming deposit, as these can override the effects of turbulence on shearing and particle segregation (e.g., Branney and Kokelaar, 2002). This mechanism operates in currents with concentrated basal parts and leads to rapid particle aggradation. The local occurrence of emlLT indicates a higher energy in the early stages of the pyroclastic current, such that it could entrain a higher proportion of dense lithics. Most ignimbrites do not show significant vertical variations, suggesting deposition under quasistable conditions, with pyroclast aggradation at a constant rate (e.g., Branney and Kokelaar, 2002). Normal lithic gradation in some sections is attributable to waning pyroclastic flows in terms of velocity, competence or mass flow. The large thickness and fine ash content of the deposits is consistent with subcritical pyroclastic flows (sensu Bursik and Woods, 1996), which are relatively slow, thick, and require a high mass flux from the source. The eutaxitic texture and moderate to dense welding of the ignimbrites indicate a high emplacement temperature. The textures of the lithic fragments denote thermal erosion, which is consistent with the high welding degree of the ignimbrites. The welding is attributable to load compaction of the cooling ignimbrites (e.g., Freundt, 1999), and it is also possible that reabsorption of volatiles (e.g., Sparks et al., 1999), favored by poor sorting, played an important role. Finally, the thickness and welding of the ignimbrites, together with the absence of Plinian fall deposits, are consistent with low, large volume eruptive columns (i.e., boiling over) linked to caldera subsidence (e.g., Branney et al., 1992; Freundt, 1999), in which an instantaneous and continuous collapse of the ejected material occurs. These eruptive columns lose less heat and fine ash by mixing with atmospheric air than high-altitude Plinian plumes (e.g., Branney et al., 1992).

VF2: Phreatomagmatic deposits (dbLT, bLT, xsT, mT, //sT, //sTves)

Description: Succession of dacitic ash-lapilli to ash tuffs, of light yellowish gray to orange and reddish color. Two groups of lithofacies can be distinguished, which form decimeter- to centimeter-scale intercalations in similar proportions (Figs. 3 and 5E) and are described next:

- 1. G1 Ash-lapilli to ash tuffs with diffuse to well-defined bedding: Dominance of diffusely bedded ash-lapilli to ash tuffs (dbLT), in some parts with well-defined bedding (bLT), which show a finer grain size compared to ignimbrites from association VF1 (fragments generally <1 cm); locally, there are intercalations of cross-laminated ash tuffs (xsT). The diffuse bedding and stratification of dbLT is defined by normal and inverse gradations in size (medium lapilli to fine ash) and proportion of fragments, which also have a directional fabric, with the long axes of the clasts parallel to the bedding plane (Fig. 5I). bLT is closely related to dbLT, differentiated by the development of abrupt bedding planes (Fig. 5H). xsT forms layers of a few centimeters thick, with low-angle cross-lamination (5-15°) and numerous internal erosive truncations (Fig. 5G).</p>
- 2. G2 Massive to laminated ash tuffs: Dominance of massive ash tuffs (mT), with minor occurrence of vesicular laminated ash tuffs (//sTves) and laminated ash tuffs (//sT) (Fig. 5F). mT consists of well-sorted vitric ash tuffs, 7-80 cm thick, mainly coarse ash size, and with vesicular texture (<10%vol.). //sTves has discontinuous horizontal lamination and a high proportion of ellipsoidal to irregular vesicles (25-30%vol.), is moderately sorted, and forms beds <30 cm thick. //sT has continuous horizontal lamination, good sorting, and forms beds 8-20 cm thick.

More specific features of both groups are found in the detail section (Fig. 5E in the main article and Table A1 in this Appendix), which comprises the last few meters toward the top of the VF2 succession, up to the onset of a new thick ignimbrite of VF1. The intercalation of a \sim 1.2 m package of the VF1 association is worth to notice, composed of the lithofacies emlLT + emLT + //sT + mT (Fig. 5H).

TABLE A1. DESCRIPTION OF THE DETAILED STRATIGRAPHIC SECTION OF FIGURE 5E.

N°	Thickness (cm)	Lithofacies	Description	Images
1	50	dbLT	Ash-lapilli tuff to ash tuff. Starts with a 10 cm-thick, clast-supported, and poorly sorted layer (average grain size of \sim 5 mm, with maximums of \sim 4 cm), rich in angular volcanic lithics (25-35%) and crystals (20-25%) of plagioclase $>$ quartz \sim amphibole, along with numerous <i>fiamme</i> (15-20%). The layer shows normal gradation to a matrix-supported domain enriched in vitreous fine ash, spanning the remaining 40 cm. Within this domain, there are numerous, rhythmically intercalated 1-5 cm thick levels that are analogous to the initial layer, with both normal and inverse grading with respect to the fine domain. The deposit has a fabric given by clasts with their long axes parallel to the stratification plane.	Fig. 5F, I
2	80	mT	Massive, well-sorted, vitric ash tuff with a coarse ash grain size and vesicular texture (5-10% vol.). It contains abundant non-oriented angular glass shards (35-45%), crystals (20-25%) of plagioclase >> quartz \sim amphibole, subangular pumice fragments (15-20%), and black volcanic lithics (8-12%). Vitreous fine ash content is low.	Fig. 5F
3	10	//sT	Vitric ash tuff with continuous horizontal lamination. It has a flat basal contact, and is richer in vitreous fine ash content compared to the tuff of level 2. The deposit has limited lateral continuity, spanning a few meters only. The fragments do not exhibit oriented fabrics.	Fig. 5F
4	20	//sTves	Vitric ash tuff with discontinuous horizontal lamination. It shows a gradational contact with the tuff of level 3 and maintains limited lateral continuity. It differs from the previous level in terms of larger grain size, moderate sorting, content of <i>fiamme</i> (<1 cm, 5-10%), and a high percentage of elliptical to irregular vesicles (25-30%vol.).	Fig. 5F
5	20	mT	$\label{thm:continuous} Vitric \ ash \ tuff, analogous \ to \ the \ previous \ one \ within \ this \ lithofacies. \ It \ has \ an \ irregular \ base.$	Fig. 5F, G
6	8-25	xsT	Well-sorted crystalline ash tuff, with a slightly irregular erosive base. It exhibits low-angle cross-lamination (5-15°) with laminae separated by numerous erosive surfaces. It consists of 50-60% crystals, predominantly plagioclase > amphibole \sim quartz, along with subordinate lithics, in a matrix of glass shards and vitreous fine ash.	Fig. 5F, G
7	12-40	emlLT	Well-sorted, massive ash-lapilli tuff with eutaxitic texture. It shows a flat to slightly erosive contact with level 6. It has a high content (35-45%) of polymictic volcanic lithics, with graded sizes up to \sim 4 cm. It also contains 15-20% <i>fiamme</i> up to 3 cm and subordinate crystals, within a vitreous matrix with incipient to moderate welding.	
8	45-73	emLT	Well-sorted, massive vitric lapilli-ash tuff with eutaxitic texture. It has a gradational basal contact, and a lower content of lithics (15-25%) and <i>fiamme</i> (8-15%) than level 7, maintaining their size range. Incipient welding is observed.	Fig. 5H
9	20	//sT	Vitric crystal ash tuff with well-defined tabular geometry and continuous horizontal lamination. It exhibits good sorting, with 1-2 mm-sized fragments, predominantly consisting of glass shards (with bubble-wall textures) and crystals, along with subordinate volcanic lithics. The fragments do not exhibit oriented fabrics.	Fig. 5H
10	15	mТ	$\label{thm:continuous} Vitric \ crystal \ ash \ tuff, very \ similar \ to \ the \ previous \ one \ in \ terms \ of \ components \ and \ geometry, \ but \ with \ a \ massive \ structure.$	Fig. 5H
11	180	dbLT; bLT	Ash-lapilli tuffs to ash tuffs. They are very similar to the initial deposit (number 1 in this section). They are differentiated by the intercalation of centimeter-thick layers with well-defined bedding planes (bLT).	Fig. 5H
12	15	mT	Massive vitric ash tuff, with coarse ash grain size.	-
13	30	emlLT	Massive ash-lapilli tuff with eutaxitic texture. Analogous to the previous layer of this lithofacies.	-
14	>200	emLT	$\label{thm:massive} \mbox{Massive vitric lapilli-ash tuff with eutaxitic texture. In gradational contact with lithofacies $emlLT$.}$	-

Description from base to top of the detailed stratigraphic section of Fig. 5E, showing the interplay between lithofacies associations VF2 and VF1 in the lower part of the Las Tetas section (see Fig. 3 for reference). Associations VF1 and VF2, as well as the groups G1 and G2 within VF2, are represented using the same colors as in figure 5E.

Interpretation: For each group of lithofacies, the following interpretations are made:

- 1. G1 Ash-lapilli to ash tuffs with diffuse to defined bedding: Diffuse structures and normal and inverse gradations, together with fine grain size and absence of welding, are typical features of deposits formed by cold and highly mobile currents related to phreatomagmatic activity (e.g., Self, 1983; McPhie, 1986), commonly known as base surge deposits (e.g., Cas and Wright, 1987). The diffuse structures suggest a granular flow mechanism in the lower part of the current, linked to a relatively high concentration in that zone, while the gradations indicate instabilities during aggradation, attributable to successive surges in a sustained turbulent current (e.g., Branney and Kokelaar, 2002). In this sense, the occurrence of bLT together with dbLT would denote locally stronger shear gradients. The xsT layers are attributed to minor pulses of slow aggradation, likely deposited by traction (e.g., Branney and Kokelaar, 2002).
- 2. G2 Massive to laminated ash tuffs: Massive ash tuffs (mT) indicate stable direct-fall processes (i.e., fallout deposits) (e.g., Talbot et al., 1994). Their vesicularity points to humid and cold conditions (<100 °C) in the presence of liquid water, which favor the entrapment of air bubbles (e.g., Walker, 1971). //sTves denotes higher humidity, given its higher vesicularity and poorer sorting, while its discontinuous lamination is attributed to water splashing during aggradation (e.g., Walker, 1971, 1981). The //sT layers indicate local episodes of laterally uniform and temporally unsteady aggradation (Branney and Kokelaar, 2002).

The intercalations of base surge and fallout deposits (e.g., Self, 1983; McPhie, 1986), and the horizontal layering and lamination (e.g., Branney, 1991), allow interpreting this association as phreatomagmatic deposits. Phreatomagmatic eruptions generate pulsational currents, sustained by rapidly depletive surges, which deposit by direct fallout from ash clouds and by traction from slightly faster pulses (e.g., Branney and Kokelaar, 2002). The relatively fine grain size of G1 ignimbrites (compared to ignimbrites from association VF1) is attributable to a higher degree of magma fragmentation resulting from mixing with surface water, which increases the explosiveness of the eruption (e.g., Self and Sparks, 1978). An origin of this kind is consistent with caldera-type volcanism, characterized by large-scale explosive silicic eruptions, which may occur in contact with lakes developed in their crater (e.g., Self and Sparks, 1978; McPhie, 1986).

The VF1 deposit interbedded in the upper part of VF2 in the Las Tetas section would have been formed by a more concentrated, slower, and hotter pulse, as indicated by the massive fabric and welding of *emlLT* and *emLT*, while the //sT and mT layers are attributed to direct fallout from the co-ignimbrite ash cloud. This episodic transition between VF2 and VF1 could be indicative of an episodic loss of the influence of water on the eruption mechanism, giving way to long-lasting drier conditions. The latter reflects a complex relationship between water availability (and access) and the morphology of the emission center (*e.g.*, Self, 1983).

VF3: Distal pyroclastic surge deposits (sT, xsT, mLT, mLTf, //sT)

Description: This association groups thin (<dm-thick) stratified pyroclastic deposits intercalated in the Las Tetas section (Fig. 3). The main package corresponds to a succession of stratified (sT) and cross-stratified (xsT) ash tuffs, and massive lapilli-ash tuffs with directional grain fabric (mLTf), brownish red in color. These lithofacies are interbedded in variable proportions, forming centimeter- to decimeter-scale layers, with common flat-erosive basal contacts in the case of sT and xsT, and gradational in the case of mLTf (Fig. 5J and K). sT and xsT are clast-supported, have moderate to good sorting, and their stratification is defined by variations in fragment size and composition. The clasts have angular to rounded shapes, and consist of plagioclase (50-55%), volcanic lithic fragments (10-15%), quartz (7-12%) and glass shards (20-25%), so the tuffs are compositionally classified as crystalline. mLTf is supported by a matrix of vitreous fine ash and glass shards and has poor sorting. It contains abundant vitreous juvenile pyroclasts (30-50%) up to 20 mm long, rounded, elongated and with diffuse edges, which form a directional fabric with their long axes parallel to the stratification plane (Fig. 5K). To a lesser extent (17-22%), it has plagioclase and quartz crystals, and subordinate volcanic lithics. These tuffs are classified as vitric in terms of fragment composition.

Other two thin, brownish-red pyroclastic deposits of this association are intercalated in the alluvial succession of association A1 (Fig. 3). The lower one (Fig. 5L) consists of a layer of massive lapilli-ash tuff (mLT) of vitric fragment composition, which towards the top acquires a directional grain fabric (mLTf) and is overlain by a parallel-stratified ash tuff (//sT), also vitric. Finally, the upper deposit is a layer of lithofacies //sT, also vitric.

Interpretation: The overall dominance of traction deposition, moderate to good sorting, and high proportion of crystals and lithics of these deposits are consistent with deposition from dilute pyroclastic density currents

(i.e. pyroclastic surges) (e.g., Cas and Wright, 1987; Branney and Kokelaar, 2002). The low thickness and fine grain size of the packages suggest deposition distal from the vent.

For the main package of this association, the contact relations and composition of the lithofacies denote a highly episodic character in their deposition, in addition to a pyroclastic segregation prior to it. A highly turbulent pyroclastic density current is inferred, with surges capable of depositing pyroclasts in different proportions, and others with sufficient energy to erode locally. The segregation of pyroclasts suggest a density stratification in the lower (basal) part of the current, which is also attributable to the turbulence of the flow (e.g., Branney and Kokelaar, 2002). This pyroclastic segregation would be responsible for the lithofacies developed, since well-sorted crystal and lithic fragments facilitate tractional deposition (sT and xsT), whereas abundant vitreous fine ash points to to fluid escape as the dominant depositional control, with a granular flow component capable of generating the directional fabric of juvenile pyroclasts observed in mLTf (e.g., Branney and Kokelaar, 2002).

As for the other two pyroclastic levels intercalated in a succession of association A1, the lower one denotes an evolution from a deposition controlled by fluid escape and granular flow (*mLT* and *mLTf*) to one dominated by ash fallout from the co-ignimbrite cloud (//sT), which can be attributed to a gradual decrease in particle concentration in the lower part of the current (*e.g.*, Branney and Kokelaar, 2002). The second pyroclastic deposit, consisting only of the //sT lithofacies, as well as the //sT level that caps the previous deposit, can be categorized as ash-cloud surge deposits (*sensu* Cas and Wright, 1987), which represent the final depositional reaches of a pyroclastic current.

2.2. Sedimentary lithofacies associations

2.2.1. Fluvial

F1: Gravel-rich braided river (Gh, Gp, Gcm, Sh1, Ss, Fm)

Description: Succession of conglomerates, gravelly sandstones, sandstones and mudrocks, all brown in color, forming meter- to centimeter-scale layers. They have an architecture strongly controlled by the contact surfaces that separate the deposits (Fig. 6A):

- 1. Bedding: Horizontal and planar, smooth, distinctly defined, and with variable lateral continuity.
- 2. Non-erosive contact: Conformable contact between two layers of different lithofacies.
- 3. Lateral truncation surface: Concave, smooth, vaguely to distinctly defined, separating laterally juxtaposed deposits of equal or different lithofacies.
- 4. Minor erosive surface: Irregular, relatively rough, vaguely to distinctly defined, and with reduced lateral continuity.
- 5. Major erosive surface: Irregular, highly rough, distinctly defined, and with high lateral continuity. Gravels make up >90% of the deposits, are up to 12 cm in diameter, rounded to subangular, and spherical to discoidal; sands appear locally in close relation to the gravels, and the mud forms subordinate levels. Compositionally, gravels and coarser sands contain abundant polymictic lavic, tuffaceous, and intrusive lithic fragments; finer sands are enriched in plagioclase, quartz and amphibole crystals, and the mud concentrates clays. Four types of deposits can be distinguished:
- 1. G1 Conglomerates with horizontal bedding: Conglomerates to gravelly sandstones with horizontal bedding (Gh), in layers a few decimeters to a couple of meters thick, with major or minor erosive basal surfaces. Bedding is defined by centimeter-scale pulses with normal gradation, and clasts are commonly imbricated. In some sectors, tabular layers up to 50 cm thick are intercalated, formed by thin (cm-thick) levels in which gravels grade to laminated sandstones (Sh1) (Fig. 6B).
- 2. G2 Conglomerates with planar cross-bedding: Conglomerates to gravelly sandstones with planar cross-bedding (Gp), in layers a few decimeters to a couple of meters thick, with major or minor erosive basal surfaces (Fig. 6B and D). Bedding is defined by centimeter-scale pulses with normal gradation. They are usually juxtaposed to other deposits by lateral truncations (Fig. 6A).
- 3. G3 Clast-supported conglomerates to poorly sorted sandstones: Massive clast-supported conglomerates (Gcm) in irregular intergradation with massive to diffusely laminated, poorly sorted sandstones (Ss). They form layers a few decimeters thick with erosive basal surfaces, which are generally of minor order (Fig. 6C and D).

- 4. G4 Massive mudrocks: Massive mudrocks to sandy mudrocks (Fm), forming layers <20 cm thick with net basal surfaces. They are interrupted by erosive surfaces, so their lateral continuity is low (Fig. 6C).
- **Interpretation:** For each type of deposit, the following interpretations are made:
- 1. G1 Conglomerates with horizontal bedding: They are indicative of tractional processes as part of the bedload (e.g., Smith, 1990), deposited in episodes of high water and sediment discharge, creating beds with vertical and frontal accretion (e.g., Miall, 2006). Their normal gradation reflects pulses of sedimentation, with deposition of finer material as the flow loses competence. The Gh + Sh1 levels could correspond to the filling of shallow channels furrowed over the forming gravel layers (e.g., Smith, 1990).
- 2. G2 Conglomerates with planar cross-bedding: Considering their structures, their lack of significant lateral or vertical variations, and their lateral truncations with other deposits, it is inferred that their sedimentation was controlled by lateral accretion at the margins of gravel bars during the migration of sinuous channels (e.g., Smith, 1990).
- 3. G3 Clast-supported conglomerates to poorly sorted sandstones: They are indicative of rapidly sedimenting bedload (e.g., Miall, 2006), so they are inferred to be scour pool fills, which is consistent with the shape and thickness of the deposits. Scour pools, along with bars, are fundamental morphological units in the dynamics of a gravel braided river (e.g., Ashmore, 1982; Thompson, 1986).
- 4. G4-Massive mudrocks: The lithology and thickness of the mudrocks and sandy mudrocks of Fm suggest deposition in shallow waters by gentle currents (e.g., Smith, 1990) or in ponded waters in abandoned channels (e.g., Miall, 2006). Therefore, they are cover deposits that close sedimentation cycles, which help explain their disposition over the other three groups of deposits.

Based on the above, this lithofacies association is interpreted as representative of a braided fluvial system with abundant gravel and sand, dominated by successive vertical and lateral accretion processes. The stacking of gravels with fine sediment intercalations suggests multistage deposition, with waning stages that would have emerged the bars and deposited fine sediments in low-energy pools, followed by floods that would have reactivated the bars, partially eroding previous deposits and accumulating gravels (*e.g.*, Smith, 1990; Miall, 2006). The features of this association are consistent with the middle to distal parts of a gravel braided river, in which the flow is distributed in several channels within a wider and relatively shallow channel, forming horizontally and cross-bedded deposits; as opposed to the proximal part, where the bedload is thicker and less mobile, forming lag deposits (*e.g.*, Hein and Walker, 1977).

2.2.2. Alluvial

A1: Distal alluvial fan (Sh1, Sh2, Gmm)

Description: Mostly composed of sandstones with planar horizontal lamination (*Sh1*), intercalated in some sections with muddy sandstones with planar horizontal lamination (*Sh2*) and massive gravelly sandstones (*Gmm*) (Fig. 3), forming deposits of light brown color with a strong reddish tone (redbeds), varying to brown and greenish. *Sh1* forms centimeter- to decimeter-scale tabular layers, which in turn form decimeter- to meter-scale sets, separated by flat to erosive surfaces (Fig. 6E and F). Its sorting is moderate to poor, and its lamination is very distinct, with internal development of normal gradation from very coarse to medium sand (Fig. 6G). The clasts are mainly subangular and spherical and consist of plagioclase and volcanic lithics to a greater extent, along with subordinate quartz and amphibole. *Sh2* is a finer grain size equivalent of *Sh1*, with medium sand- to mud-sized clasts. It is arranged in tabular centimeter- to decimeter-scale layers with flat conformable bases, which are intercalated with those of *Sh1* at different scales, configuring meter-scale sets in which one lithofacies is dominant over the other (Fig. 6E). *Gmm* forms tabular to lenticular layers of 25 cm to 1 m, with conformable to erosive bases (Fig. 6H). It contains clasts of up to 20 cm in diameter in a fine to coarse sand matrix, the larger ones with their long axes parallel to the stratification plane. They are rounded to angular, of lavic and tuffaceous type, and make up 15-35% of the layer volume.

Interpretation: The geometric arrangement of the deposits and their sedimentary structures are consistent with an origin resulting from unconfined flows or sheetfloods in the distal portion of an alluvial fan, or in an alluvial plain, linked to catastrophic sediment-laden flooding (*e.g.*, Blair and McPherson, 1994; Collinson, 1996; Nichols, 2009). Sheetfloods dominate over debris flows in fans whose inputs are clay-poor (*e.g.*, Blair and McPherson, 1994), which is consistent with the low mud content of these deposits. Marginal sands of

alluvial fans are deposited by supercritical flows with reduced competence due to a lower slope in that area (e.g., Blair and McPherson, 1994). This is consistent with the tabular geometry and horizontal lamination of the sandstones, and the rhythmic intercalation of coarser and finer sediments. The gravelly sandstones (Gmm) represent higher energy events, probably hyperconcentrated sheetfloods, as suggested by their directional grain fabric, tabular shape, and intercalation with finer sediments (Sh1) (e.g., Collinson, 1996).

2.2.3. Lacustrine

L1: Carbonate lacustrine (Ll, Fl)

Description: Decimeter-scale deposits of calcilutites and subordinate calcarenites with fine horizontal lamination (Ll). In the El Tapado section, centimeter-scale layers of laminated mudrocks to fine-grained sandstones (Fl) are intercalated (Fig. 7A). In this section, Ll deposits have a gray color varying to light brown on the altered surface. Under the microscope, it is observed that calcilutites are composed mostly of micrite-rich laminae, with intercalated thin laminae rich in siliciclastic fragments and dispersed volcanic glass shards (Fig. 7C). Other interlaminated layers consist of a pellet framework, with abundant sparitic cement as binder (Fig. 7C). In turn, lithofacies Fl is essentially composed of crystals, volcanic lithics, and clay. In the Ingaguás section, lithofacies Ll comprises deposits of laminated calcilutites and subordinate calcarenites, which form well-bedded, <30 cm-thick layers light brown in color (Fig. 7B). Under the microscope, the calcilutites are composed mostly of micrite along with skeletal fragments, pellets and clay, the proportion of which varies between laminae (Fig. 7D and E). Other laminae are composed of fine sand-sized crystals and lithics in a clayey matrix. The skeletal fragments consist of remains of very small (<500 μ m) and thin concave shells, as shown in figure 7E and F.

Interpretation: The uninterrupted horizontal lamination and sediment composition of *Ll* suggest an origin in a carbonate lacustrine environment, controlled by the settling of suspended biogenic calcareous material from a relatively shallow body of water under low energy conditions (*e.g.*, Talbot and Allen, 1996). The *Fl* levels intercalated in the El Tapado section denote local siliciclastic inputs to the lake at a sufficiently low rate for carbonate sedimentation to prevail (*e.g.*, Nichols, 2009). This enabled the preservation of glass shards, which are indicative of contemporary volcanic activity. In the Ingaguás area, the variable proportion of skeletal fragments between calcilutite laminae suggests recurrent changes in environmental conditions that control the proliferation of these organisms. The size, shape and thickness of these fragments indicate that they would correspond to freshwater organisms, probably branchiopods or ostracods; these taxa are common in shallow continental lacustrine basins (*e.g.*, Gallego and Breitkreuz, 1994).

L2: Deep lacustrine volcaniclastic (Sm, Fm, Fl, Rp)

Description: Rhythmic centimeter- to decimeter-scale intercalations between massive to diffusely laminated sandstones (Sm) and laminated to massive mudrocks (Fl and Fm), greenish to brownish gray in color. They are rich in volcanic clasts, and form layers up to ~1.5 m thick (Fig. 8A). Sm has flat, conformable to erosive bases, and commonly develops normal gradation from very coarse to fine sand (Fig. 8B). In general, it is composed of crystals (plagioclase and sparse amphibole), volcanic lithics and subordinate vitroclasts, has moderate to good sorting (in ungraded layers), and low to medium roundness and sphericity. Other levels are richer in fine gravel-sized vitroclasts, which inflict poor sorting, coincident with a poorer roundness and sphericity. Fl and Fm are composed of fine vitreous ash and glass shards, with sparse crystals. Small synsedimentary folds develop in some of the rhythmic layers described (Fig. 8C). Locally, layers composed of vitroclasts and plagioclase crystals with preserved pyroclastic textures (i.e., redeposited pyroclastic deposits) are intercalated, displaying a faint horizontal lamination (Rp; Fig. 8D).

Interpretation: The lithofacies described and their configuration are consistent with sedimentation by turbidity currents in a deep lacustrine environment, a mechanism in which the denser, coarser fraction is deposited from the head and body of the flow as a massive layer with variable gradation, and gradually transitions to a fine-grained layer deposited from the suspended entrainment cloud (*e.g.*, Cas and Wright, 1987; Nichols, 2009). The poor sorting of some layers is explained by density contrasts of the volcanic material, rather than by poor hydraulic sorting only (*e.g.*, Cas and Wright, 1987). Synsedimentary folds are attributable to slumps, common in turbiditic environments (*e.g.*, Elliott and Williams, 1988). The texture and composition of fragments suggest relatively short transport prior to lake entry. The redeposited pyroclastic

deposits imply contemporaneous volcanic activity nearby, being their faint lamination consistent with a decantation mechanism.

L3: Shallow lacustrine volcaniclastic (Swr, Fl, Rp)

Description: Millimeter- to centimeter-scale intercalations between laminated mudrocks (Fl) and fine-grained sandstones with wave ripples to sinuous lamination (Swr) (Fig. 8E), brownish to greenish light gray in color, forming decimeter-scale strata. They develop wavy bedding and flaser bedding (Fig. 8F and G), and are composed essentially of fine vitreous ash (Fl) and feldspar crystals (Swr). The mudrocks show mottled colors in shades of green, red, and yellow. In some sectors, there are intercalated redeposited pyroclastic deposits (Rp) a couple of decimeters thick, showing a massive structure and composed of crystals and vitroclasts of coarse ash grain size (Fig. 8G).

Interpretation: The association of wave-rippled sand and laminated mud represents an alternation of tractional transport by oscillatory flows and decantation of mud from suspension, which can be linked to a shallow lacustrine environment (*e.g.*, Rajchl *et al.*, 2008; Nichols, 2009; Melchor *et al.*, 2012). Mottling of mud is attributable to pedogenic processes, common in this type of environment (*e.g.*, Tucker, 2003). The redeposited pyroclastic deposits denote contemporaneous volcanic activity nearby, and their massive structure is consistent with the inability of the waves to form structures, given their grain size.

2.2.4. Saline lacustrine to subaerial

LS1: Saline lacustrine volcaniclastic with occasional sheet floods (Swr, Fl, Fm, Ec, Sm)

Description: Succession dominated by sets of thinly (<dm-thick) bedded laminated to massive mudrocks to sandy mudrocks (*Fl* and *Fm*), wave-rippled to sinuously laminated sandstones (*Swr*), and evaporitic calcite (*Ec*), in which meter-scale packages of tabular layers of massive sandstones (*Sm*) are interbedded (Fig. 9A). The *Fl-Fm+Swr+Ec* layers are millimeter to centimeter-thick and develop wavy bedding and lenticular bedding (Fig. 9B). In general, layers are continuous, and the mudrocks are laminated (*Fl*) (Fig. 9B). In other sectors, these sets show cut-and-fill structures with semi-consolidated disaggregated sands, and the mudrocks are massive (*Fm*) (Fig. 9B). *Fl* and *Fm* are reddish brown, composed of fine glass and sparse crystals. *Swr* is light greenish gray, has fine to medium grain size, moderate sorting, and angular grains, corresponding mostly to feldspars and volcanic lithics, with carbonate cement as binder. *Ec* has a crystalline texture, with medium-grained polygonal aggregates of calcite. *Sm* is dark gray to greenish gray in color, forming <50 cm-thick layers of moderately sorted, very coarse- to fine-grained sand, angular to subangular and subprismoidal to subdiscoidal, and commonly show normal gradation (Fig. 9C). *Sm* is composed mostly of feldspars, together with volcanic lithics, quartz, and scarce amphibole.

Interpretation: Fl and Swr indicate shallow lacustrine sedimentation (as in association L3), and the intercalation with numerous evaporite levels (Ec) points to a saline lake environment. This implies that the evaporation rate must have exceeded the inflow, which occurs in arid or semi-arid climates, and that the basin must have been hydrologically closed or with restricted drainage (e.g., Eugster and Hardie, 1978). Variations in shape, continuity and structures in the lithofacies are attributed to varying degrees of energy of the density currents responsible for the sand inputs. Evaporite production would have been controlled to a greater extent by the frequency of clastic inputs to the lake (e.g., Hardie et a., 1978), which may have a seasonal control although are more commonly irregular (e.g., Hardie et a., 1978; Nichols, 2009). As for the massive sandstones (Sm), their tabular geometry and normal gradation indicate tractional deposition by waning pulses from unconfined high-energy flows (e.g., Benvenuti, 2003). The texture of the grains suggests reduced transport prior to deposition, and the massive to diffusely laminated structure points to rapid deposition due to high flow concentration or abrupt loss of flow competence. Therefore, these deposits are interpreted as the product of unconfined flash floods, which would have occurred during subaerial exposure stages. This is consistent with the activity of ephemeral river courses during heavy rains, although an alluvial origin cannot be completely ruled out.

LS2: Sheet floods and ephemeral lakes (Sm, Fl, Ec, Eg)

Description: Packages of decimeter-scale massive sandstones (*Sm*) in the upper part of the El Tapado section, intercalated towards the top of the succession with decimeter-thick packages of laminated mudrocks to sandy mudrocks (*Fl*) with evaporitic calcite (*Ec*) lenses, culminating with a meter-scale package of

gypsum (Eg). Sm is grayish green to light brown, has moderate to poor sorting, with mostly medium to very coarse-grained sands (and subordinate fine gravel), and ~5% mud. It has pulses of normal gradation that define a diffuse lamination (Fig. 9D and G). The clasts are subangular and spherical, and consist mainly of plagioclase, together with volcanic lithics, mafic minerals and subordinate quartz. Fl has a brownish color, and forms millimeter- to centimeter-thick layers of sinuous shapes, conditioned by the shape of the evaporite lenses. It comprises fine to very fine sand, consisting of feldspars to a greater extent, plus mafic minerals, volcanic lithics and quartz, with ~15% mud. It has horizontal lamination, given by gradations between the described components (Fig. 9H). Ec forms millimeter- to centimeter-thick lenses with crystalline texture, conformed by fine-grained polygonal aggregates. Eg is found forming centimeter- to meter-thick layers, with subordinate fine sediments; it also has a crystalline texture, composed of medium-grained tabular aggregates. Figures 9E and F show an outcrop and a detail section of these deposits, respectively, in the uppermost 30 m of the El Tapado section.

Interpretation: As in association LS1, the tabular packages of *Sm* would have been formed by unconfined, high-energy flash floods spread over a plain under subaerial conditions (*e.g.*, Benvenuti, 2003). In turn, the *Fl* and *Ec* deposits are inferred to be the product of sedimentation in ephemeral lakes, which are temporary bodies of water formed in arid areas by occasional heavy rains and are characterized by repeated cycles of flooding and evaporation that give way to rhythmic thin layers of fine sediments and evaporites (*e.g.*, Hardie *et al.*, 1978; Lowenstein and Hardie, 1985). Flash flood and ephemeral lake deposits are a characteristic association of arid depositional environments (*e.g.*, Nichols, 2009). The succession of thick layers of *Eg* that crowns the section is attributed to a final stage of advanced chemical sedimentation, which allowed the precipitation of more soluble minerals.